

NASA TECHNICAL NOTE

NASA TN D-5673



NASA TN D-5673

CASE FILE COPY

STEADY-STATE ANALYSIS OF A BRAYTON SPACE-POWER SYSTEM

by John L. Klann

Lewis Research Center
Cleveland, Ohio

NATIONAL AERONAUTICS AND SPACE ADMINISTRATION • WASHINGTON, D. C. • FEBRUARY 1970

1. Report No. NASA TN D-5673	2. Government Accession No.	3. Recipient's Catalog No.	
4. Title and Subtitle STEADY-STATE ANALYSIS OF A BRAYTON SPACE-POWER SYSTEM		5. Report Date February 1970	
		6. Performing Organization Code	
7. Author(s) John L. Klann		8. Performing Organization Report No. E-5281	
9. Performing Organization Name and Address Lewis Research Center National Aeronautics and Space Administration Cleveland, Ohio 44135		10. Work Unit No. 120-27	
		11. Contract or Grant No.	
		13. Type of Report and Period Covered Technical Note	
12. Sponsoring Agency Name and Address National Aeronautics and Space Administration Washington, D. C. 20546		14. Sponsoring Agency Code	
15. Supplementary Notes			
16. Abstract An experimental system was approximated in a digital computer study. Parametric and simulated-fixed-system operations to be conducted in ground tests were examined, mainly to show trends in conversion efficiency. With the design working-gas mixture of helium and xenon, and with temperatures at their design values, system conversion efficiency was estimated to increase from about 0.14 at 2 kilowatts of electric output to about 0.24 in the 10- to 15-kilowatt range.			
17. Key Words (Suggested by Author(s)) Analysis Brayton Power		18. Distribution Statement Unclassified - unlimited	
19. Security Classif. (of this report) Unclassified	20. Security Classif. (of this page) Unclassified	21. No. of Pages 59	22. Price * \$3.00

*For sale by the Clearinghouse for Federal Scientific and Technical Information
Springfield, Virginia 22151

CONTENTS

	Page
SUMMARY	1
INTRODUCTION	1
POWER SYSTEM DESCRIPTION	3
Test Configuration	3
Heat source	3
Rotating machinery	3
Recuperator and gas-to-liquid heat exchangers	3
Electrical subsystem	3
Heat-rejection subsystem	3
Gas management subsystem	5
System Design Conditions	5
Present Hardware Limits	6
METHOD OF ANALYSIS	7
Gas Loop and Output Power Calculations	7
Liquid-Coolant-Loop Calculations	8
RESULTS AND DISCUSSION	8
Parametric System Operation	9
Gas inventory effects	9
Turbine-inlet temperature effects	13
Compressor-inlet temperature effects	15
Operation with krypton	15
Gas-mixture relative helium mass effects	17
Simulated Solar Operation	18
Simulated Radioisotope Operation	20
Reset Compressor-Diffuser Vanes	22
CONCLUDING REMARKS	24
SUMMARY OF RESULTS	25
APPENDIXES	
A - SYMBOLS	27
B - DETAILS OF COMPUTER PROCEDURES	31
C - COMPONENT MODELS	35
REFERENCES	57

STEADY-STATE ANALYSIS OF A BRAYTON SPACE-POWER SYSTEM

by John L. Klann

Lewis Research Center

SUMMARY

An experimental Brayton space-power system was approximated in a digital computer study. Parametric and simulated-fixed-system operations to be conducted in the experimental system ground tests were examined. The study shows trends in system conversion efficiency for both design and off-design operating conditions. The analysis is independent of operational limits. However, the present limitations of the existing hardware are discussed.

With the design working-gas mixture of helium and xenon, and with temperatures at their design values, estimated levels of system conversion efficiency increased from about 0.14 at 2 kilowatts of output to about 0.24 in the 10- to 15-kilowatt range. Changes in conversion efficiency with off-design turbine- and compressor-inlet temperatures were calculated. Each inlet temperature was individually varied while the other was maintained at its design value. System conversion efficiency was insensitive to ± 20 percent changes in the relative amount of helium in the gas mixture. However, the use of krypton in place of the design gas mixture resulted in up to a 0.03 decrease in conversion efficiency.

Study of simulated radioisotope-power-system operations showed that bleeding working gas would be an effective means to maintain high system power outputs during the decay of a short-lived isotope.

Future power system gains could be achieved by modifying the compressor-diffuser vane angle for peak compressor performance. With the modified diffuser, the analysis showed conversion efficiency gains of 0.01 at the 2-kilowatt power level and of 0.02 in the 10- to 15-kilowatt range.

INTRODUCTION

Lewis Research Center has been advancing closed-Brayton-cycle technology for space electric-power-generation systems since about 1963. Current efforts are cen-

tered on a Brayton power system intended for the output power range from 2 to 10 kilowatts. The system has a design-life goal of 5 years. Its design working gas is a mixture of helium and xenon at the molecular weight of krypton, 83.8. Within the closed system, a single-shaft assembly of small rotating machinery, supported by gas bearings, operates at a controlled speed of 36 000 rpm (3770 rad/sec) and produces electric power at 1200 hertz.

The cycle operating parameters for this system were selected in reference 1 on the basis of minimizing total system weight with a radioisotope heat source. The weight of the radioisotope heat source and its shield was dominant. To keep the source size and weight low, the Brayton-cycle operating parameters were chosen to favor efficiency at the expense of increased specific radiator area (ft^2/kW) for cycle waste-heat rejection. Although the system design conditions were selected for a radioisotope heat source, the system could be mated to either a nuclear reactor or a solar-heat collector.

Lewis is currently ground testing this 2- to 10-kilowatt power system. Hardware components for the system were built under contracts with the aerospace industry. Reference 2 describes the components and the intended system ground-test configurations. In addition to the system tests, several of the major components and subsystems are being investigated separately. References 3 to 6 present some of these results. The first system ground test is using a radiant electric heat source for parametric study of system performance and to simulate both solar- and radioisotope-power-system operation. The ground testing also simulates system space-heat rejection with the use of test-facility support equipment.

The electrically heated ground-test configuration was approximated in a digital computer study of its design and off-design operation. Initial results of this study are presented herein. The power system configuration was synthesized. Where measured component performance was not available, design predictions were used. Approximate heat-transfer and pressure-drop relations were developed, fitted to the component performance, and used in the analysis.

Prior to presenting the analytical results of the study, the present power system is described, and present limitations of the existing hardware are discussed. However, the analysis itself was made independent of any system limits, and output power ranges from 2 to about 15 kilowatts were examined.

The study was made mainly to show the trends in system conversion efficiency to be expected from the ground-test configuration. Ranges in turbine-inlet temperature, compressor-inlet temperature, and the relative helium mass in the working-gas mixture were examined. The use of krypton in place of the design gas mixture was studied. Calculations were made for simulated solar- and radioisotope-power-system operation. A promising future change to the compressor-diffuser vane angle was studied for its effect on system operating conditions.

POWER SYSTEM DESCRIPTION

Test Configuration

Figure 1 is a schematic diagram of the system test configuration. The station numbers and all symbols are defined in appendix A.

Heat source. - The heat source consists of two planar banks of quartz lamps with a central, U-tube heat exchanger. This heater can be operated in either a constant-turbine-inlet-temperature mode for parametric studies and simulation of a solar-heat-collection system, or in a constant-gas-thermal-input mode to simulate a radioisotope heat source.

Rotating machinery. - The rotating machinery (turbine, alternator, and compressor) forms a single-shaft assembly that is supported by gas bearings. The machinery is designed for constant-speed, steady-state, operation at 36 000 rpm (3770 rad/sec). The turbine and compressor are single-stage, radial-flow machines, and the alternator rotor is a solid, brushless, four-pole machine of the Lundell type. A speed control and a parasitic, resistive load are used to maintain a constant output frequency of 1200 hertz and to absorb unused power. A regulator maintains the three-phase voltage at 120 volts, line-to-neutral, or 208 volts, line-to-line.

Recuperator and gas-to-liquid heat exchangers. - In addition to the source heat exchanger, there is a recuperator and a gas-to-liquid, heat-sink, heat exchanger (or waste heat exchanger) in the closed working-gas loop. The recuperator is a single-pass, counterflow heat exchanger with plate-fin surfaces. The waste heat exchanger has a cross-counterflow arrangement with plate-fin surfaces for both flows. The liquid coolant makes eight passes across the straight-through gas flow. There are two separate and completely independent liquid circuits, only one of which is to be used at any given time.

Electrical subsystem. - The electrical subsystem includes the speed control, the voltage regulator, the parasitic load, a direct-current power supply, two direct-current to 400-hertz inverters, and a signal conditioner. During steady-state power system operation, the direct-current power supply rectifies part of the alternator output to provide internal needs at ± 28 volts. Direct-current power is used by the engine controls, the signal conditioner, and by either of the two inverters. The function of the inverter is to provide 400-hertz power to a motor driving a liquid pump in the heat-rejection subsystem.

Heat-rejection subsystem. - The heat-rejection subsystem contains dual coolant loops, each with a separate motor-driven pump. The two completely independent loops provide total cooling redundancy. The coolant is dimethyl polysiloxane, $(CH_3)_3Si[OSi(CH_3)_2]_3OSi(CH_3)_3$, a silicone liquid with a room-temperature viscosity of

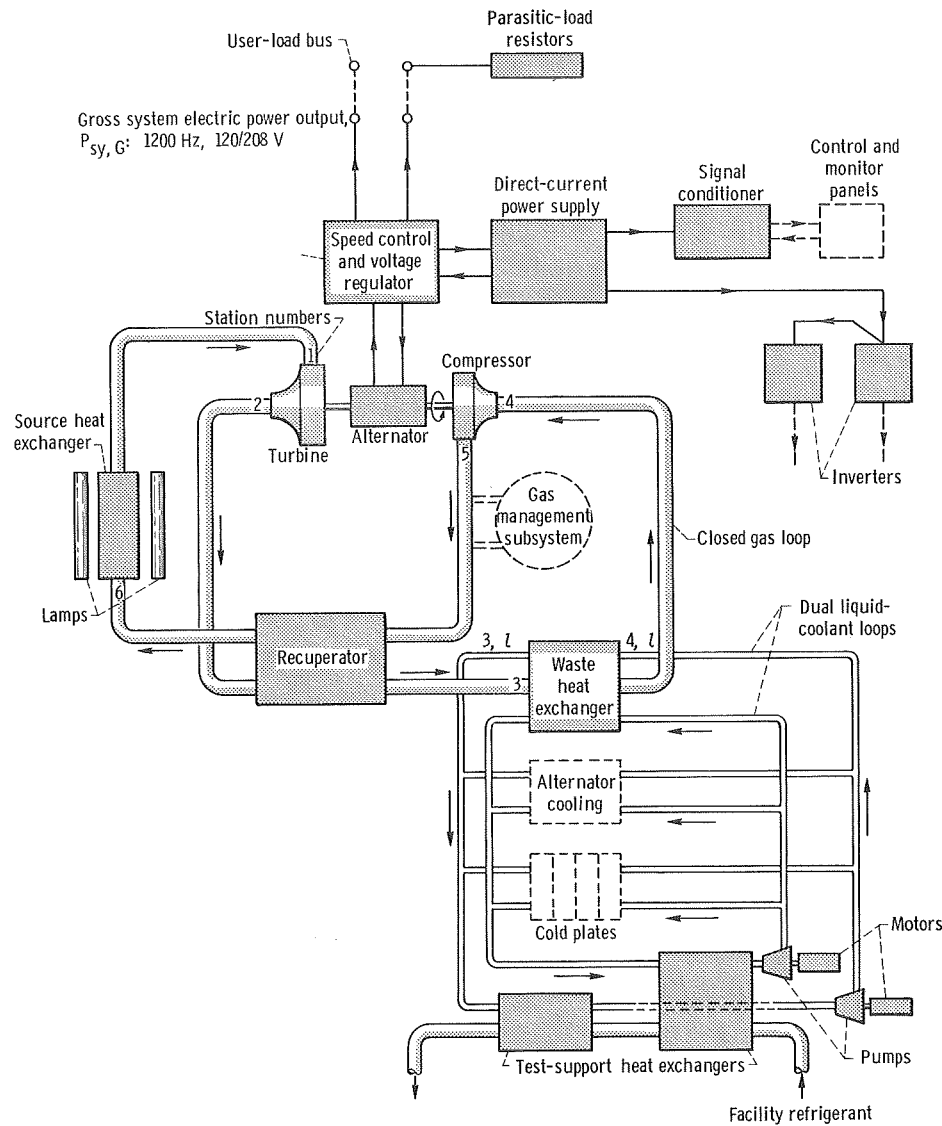


Figure 1. - Schematic diagram of Brayton-power-system test configuration.

2 centistokes ($2 \times 10^{-6} \text{ m}^2/\text{sec}$). In the test arrangement, the liquid cools three components in parallel (see fig. 1). They are the waste heat exchanger, the alternator, and a series of four flat-plate heat exchangers (or "cold plates"). Electrical subsystem components are mounted on these cold plates. The three flows mix at the exchanger outlets and pass through one of two test-support heat exchangers. After being cooled, the liquid returns to the pump for recirculation. All of the flow from each pump goes through the pump-motor cavities to cool the motor and lubricate its bearings.

The test-support heat exchangers and facility cooling supply, along with a dynamic controller, provide variable waste-heat-rejection capacity. The controller can be used to provide facility cooling in either of two modes. One mode results in a constant

compressor-inlet gas temperature. This mode will be used for the study of system parametric operation. The other mode results in waste-heat-exchanger, liquid-coolant temperatures that would occur in space with a fixed-area radiator. This mode will be used for the study of simulated solar- and radioisotope-power-system operation.

Gas management subsystem. - The gas management subsystem supplies and controls the power system working gas. It is used during power system starts and stops and for gas inventory control.

System Design Conditions

Table I shows the parametric values used in the power system component designs. All of these values, except for compressor specific speed, were taken from reference 1. The design compressor specific speed of 0.698 was used, rather than the value of 0.775 given in reference 1. This resulted in increased working-gas supply pressure levels available to the machinery bearings for self-acting operation.

Any power system must, on demand, be capable of producing power from zero to its rated output. The rated output of a closed-cycle Brayton system may also be adjusted by changing the working-gas inventory. Gas inventory, pressure level, and mass-flow rate are proportional to each other. With a constant shaft speed, the shaft work and alternator output are proportional to the gas mass-flow rate. Hence, by setting the gas pressure level the rated output of the system may be adjusted.

All components for this power system were designed to operate over the system output power range from 2 to at least 10 kilowatts. The design compressor-outlet pressure range, at a constant pressure ratio, was from about 14 to 45 psia (97 to 310 kN/m² abs). These pressures were calculated to result in from 2 to 10 kilowatts of system output power. The design effectiveness parameters (table I) and pressure drops for the recuperator and waste heat exchanger were used at the estimated 10-kilowatt, gas-loop conditions. However, in contrast to the rotating-machinery maximum design pressure

TABLE I. - DESIGN PARAMETER LIST

Working gas	Helium and xenon mixture
Working-gas molecular weight	83.8
Turbine-inlet temperature, $^{\circ}\text{R}$ (K)	2060 (1144)
Compressor-inlet temperature, $^{\circ}\text{R}$ (K)	540 (300)
Shaft rotational speed, rpm (rad/sec)	36 000 (3770)
Compressor pressure ratio, r_C	1.90
Compressor specific speed, N_s, C	0.698
Cycle-loss pressure ratio, r_T/r_C	0.92
Recuperator effectiveness, E_r	0.95
Waste-heat-exchanger effectiveness, E_w	0.95
Waste-heat-exchanger capacity-rate ratio, C_w	0.87

of 45 psia, the maximum heat-exchanger design pressure was 56 psia ($386 \text{ kN/m}^2 \text{ abs}$) at the recuperator cold-side inlet.

The rotating machinery, recuperator, and waste heat exchanger were designed for continuous, high-temperature operation over a 5-year period.

Present Hardware Limits

For system operation at design temperatures and at constant machinery rotational speed, the limits on existing components are functions of gas pressure level and time. However, these operational limits are not yet well defined. The low-pressure (or low-power) operational limit would be due to insufficient bearing-cavity pressure for self-acting operation. This limit is not time dependent. For now, it is assumed that the low-pressure limit is at the minimum machinery design operating pressure level, which corresponds to a compressor-outlet pressure of about 14 psia ($97 \text{ kN/m}^2 \text{ abs}$) and a power output of 2 kilowatts.

The high-pressure (or high-power) operational limit would probably be due to (1) limited capability for alternator cooling, (2) limited thrust-bearing capacity, or (3) a structural limit in the heat exchangers. Each of these potential limits may occur, in turn, at particular values of high operating gas pressure levels. Both alternator-cooling limits and heat-exchanger-structural limits are time dependent. Examination of design information and preliminary component test results indicates that for the system design-life goal of 5 years, a limit on alternator heating would occur first.

Based on unpublished statistical data for alternators with similar windings and potting compounds, a 5-year life corresponds to a winding temperature of about 490 K. Alternator tests in room-temperature air (ref. 4) showed that the winding hot-spot temperature increased as the load power factor was reduced from 1.0 to 0.75. At a gross alternator output of 13.4 kilowatts with a power factor of 0.75, the hot-spot temperature did not reach more than about 460 K. However, the machinery design environment was not duplicated.

Preliminary, unpublished results from a test of a single set of the rotating machinery at design conditions showed that the alternator hot-spot temperature reached 493 K at 11.4 kilowatts of gross alternator power with a load power factor of about 1.0. The corresponding compressor-outlet pressure, about 38 psia ($262 \text{ kN/m}^2 \text{ abs}$), was below both the machinery and heat-exchanger maximum design pressures. The machinery test was continued at design cooling flow conditions until, at a gross alternator power output of about 12.7 kilowatts, the alternator hot-spot temperature reached 513 K. Estimated winding potting compound life at 513 K would be about 1 year. With additional cooling,

a gross alternator output of 15 kilowatts with a hot-spot temperature of about 530 K was obtained in the machinery test.

A theoretical check on the load capacity and film thicknesses of the thrust bearing showed its operation to be practical but marginal at a compressor-outlet pressure of 56 psia (386 kN/m^2 abs), the maximum heat-exchanger design pressure. Preliminary test results, however, have indicated lower-than-design thrust loads, so thrust-bearing operation above 56 psia (386 kN/m^2 abs) may be practical. Analytically, the power system was not explored above 65 psia (449 kN/m^2 abs).

METHOD OF ANALYSIS

A digital computer program was developed to study the steady-state operation of the electrically heated ground-test power system. The configuration was synthesized. Data from individual rotating-machinery component tests were used. Performance maps for the turbine were from Nusbaum and Kofskey's results (ref. 3). Alternator efficiency was obtained from Repas and Edkin's work (ref. 4). The compressor performance maps were obtained from unpublished results of tests conducted at Lewis. Mathematical models were developed for the heat-transfer components. These models were fitted to either design predictions or to design predictions modified by acceptance test results. Details of the computer methods are presented in appendix B. Component mathematical models and their use are presented in appendix C.

The analysis was made independent of any system limits over output power ranges from 2 to about 15 kilowatts. The entire analysis was made only at the design machinery physical speed of 36 000 rpm (3770 rad/sec). Perfect insulation was assumed, so there was no heat leakage from the ducting, heat exchangers, or rotating-machinery housing. Component performance, used as the basis for the analysis, did not include the effects of flow maldistributions due to system ducting. Hence, uniform gas-flow distributions were implied in the analysis.

Gas Loop and Output Power Calculations

For each computer calculation, the closed gas loop was constrained to satisfy values of turbine-inlet temperature, compressor-inlet temperature, and working-gas inventory. With these constraints a series of iterations was needed (appendix B). Each calculation located those points on the turbine and compressor performance maps which satisfy the closed-loop pressure drops. During the course of finding the operating conditions, both the required ideal thermal input to the gas in the source heat exchanger

and the gross shaft power were determined. The gross shaft power includes a penalty for shaft-seal losses (appendix C) but not bearing friction (eq. (C34)) and alternator windage losses (eq. (C32)), which are subtracted from the gross shaft power. The gross alternator output was calculated (appendix C) for an electromagnetic efficiency corresponding to a load power factor of 0.75. Internal system electric power needs were approximated (appendix C and eq. (C100)) and subtracted from the gross alternator output to obtain the gross system output power $P_{sy,G}$. Gross system output power is defined as the sum of the three-phase, 1200-hertz power available at the parasitic- and user-load bus (see fig. 1).

Liquid-Coolant-Loop Calculations

The heat loads from the alternator cooling and the electronic-component cold plates (fig. 1) were not included in the analysis. These heat loads require lower coolant-outlet temperatures than that from the waste heat exchanger (ref. 2). In a space version of the power system, a user might reject these heat loads and further power-conditioning heat loads in a low-temperature radiator. The alternator and cold-plate cooling needs do not affect the power output calculations and are beyond the scope of this analysis.

For the study of parametric system operation, the compressor-inlet temperature, turbine-inlet temperature, and gas inventory were assigned for each calculation as independent parameters. After gas loop conditions were satisfied, the coolant mass-flow rate was calculated over a range of values (appendix B). At each value of coolant mass-flow rate, the particular values of waste-heat-exchanger coolant-inlet and outlet temperatures which would satisfy the fixed gas-side temperatures were calculated. The fixed heat load and required coolant temperatures, modified by an allowance for pump-motor cooling, were used to calculate prime space-radiator area needs (appendix C).

For the study of simulated solar- or radioisotope-system operation, the compressor-inlet temperature was constrained by assigning fixed values for prime space-radiator area and coolant mass-flow rate. Turbine-inlet temperature and gas inventory were also assigned for each calculation. Additional iterations between the gas and liquid loops were needed (appendix B).

RESULTS AND DISCUSSION

The study results are presented mainly to show trends in conversion efficiency η_{cnv} to be expected from the system ground-test configuration. Calculations were extended beyond design conditions to indicate system potential performance. A promising future

change to the compressor-diffuser vane angle was studied for its effect on system operating conditions. The results are independent of current hardware limits (see p. 6).

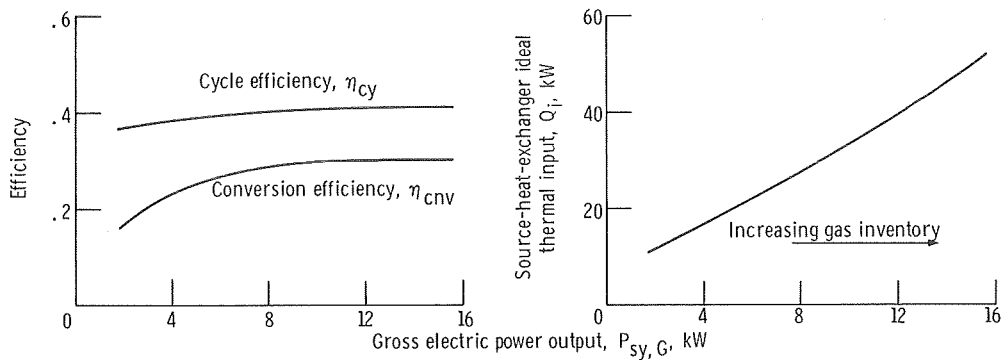
Parametric System Operation

Parametric effects on system power output and conversion efficiency were studied one at a time. The following parameters were maintained at their design conditions (table I) unless they themselves were being studied: turbine-inlet temperature, compressor-inlet temperature, working gas, and gas-mixture molecular weight. Working-gas inventory, as an independent variable, was studied over a range from 0.4 to 1.6 pounds mass in steps of 0.4 (0.18 to 0.73 kg in steps of 0.18) for each set of assigned parametric values. Results, however, are plotted against gross system output power. Gross output includes that part of the system power which would be dissipated in the parasitic-load resistors (fig. 1). For initial power system operation, 500 watts are maintained in the parasitic load to accommodate variations in system operating parameters. For the calculation of space-radiator area needs, an effective radiator heat-sink temperature of 450° R (250 K) was assumed. This sink temperature corresponds to a cylindrical radiator formed around a vehicle whose axis is oriented along its path in a low Earth orbit (ref. 7).

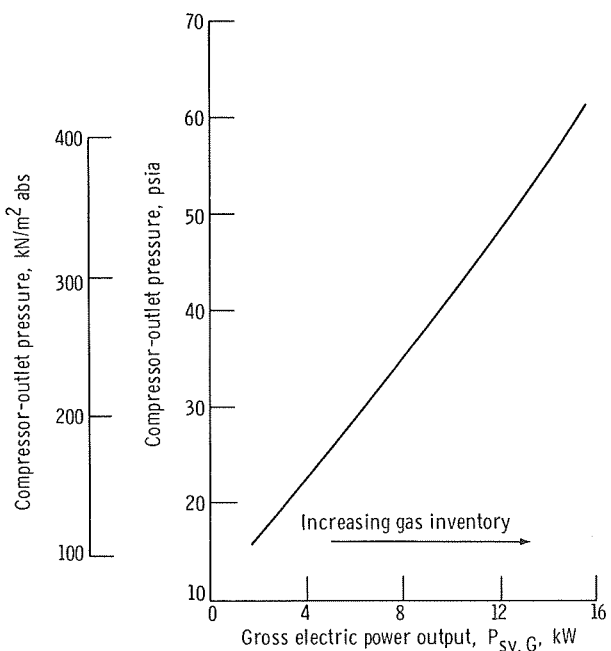
Gas inventory effects. - Figure 2 presents the effects of gas inventory on system operating conditions. Increasing gas inventory resulted in increased gas pressure and electric power output. The gas-inventory range resulted in from 1.7 to 15.6 kilowatts of output. To maintain the design turbine-inlet temperature, increased heat-source input was needed with increased output.

Figure 2(a) shows the required heat-source, heat-exchanger, ideal thermal input Q_i , cycle efficiency η_{cy} , and conversion efficiency η_{cnv} plotted against power output. Cycle efficiency was 0.37 at 2 kilowatts of output power. It increased to about 0.41 in the range from about 10 to 15 kilowatts. The relatively small change in cycle efficiency is a result of compensating changes in component performance (explained in more detail later in this section). With increasing power output, compressor and turbine efficiency and cycle-loss pressure ratio r_T/r_C increased, while recuperator effectiveness decreased. The combined positive effect of turbomachinery efficiency and cycle-loss pressure ratio exceeded the effect of the reduction in recuperator effectiveness. This accounts for the rise in cycle efficiency with increasing output power.

Conversion efficiency was 0.17 at 2 kilowatts of output power. It rose to about 0.30 in the range from about 10 to 15 kilowatts. Conversion efficiency showed a larger change than cycle efficiency because of the added losses from the alternator and system controls. At the lower power levels, these losses are a larger percentage of the output power. Above about 10 kilowatts, conversion efficiency was nearly constant. Conver-



(a) Thermal input needs for electric power output; cycle and conversion efficiency.



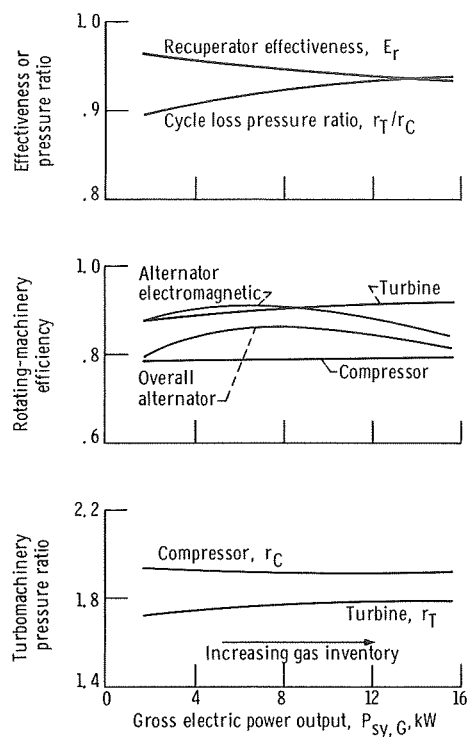
(b) Pressure-level changes with gross power output.

Figure 2. - Effects of gas inventory on system operation at design conditions. Turbine-inlet temperature, 2060° R (1144 K); compressor-inlet temperature, 540° R (300 K); working gas, helium-xenon (molecular weight, 83.8).

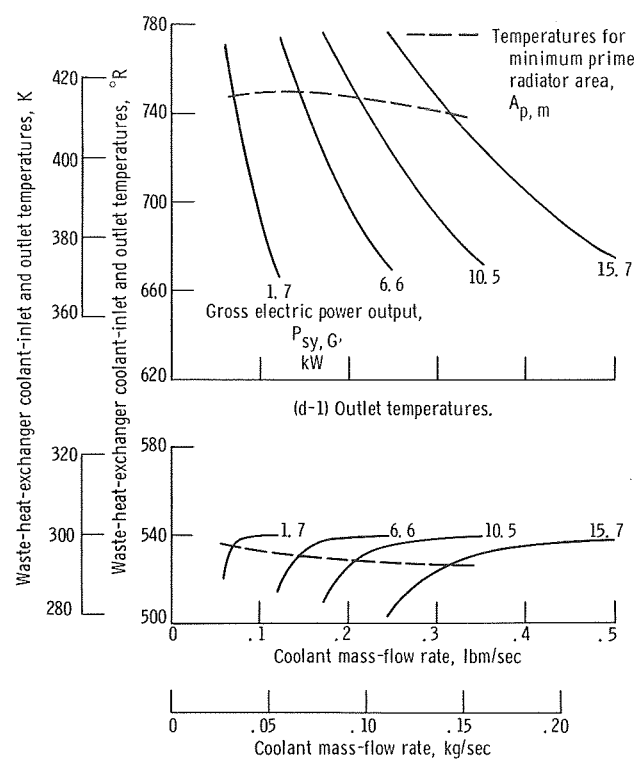
sion efficiency did not continue to increase because of rapidly increasing alternator electromagnetic losses.

Due to the combined component effects, the required source-heat-exchanger thermal input (fig. 2(a)) was not linear with power output.

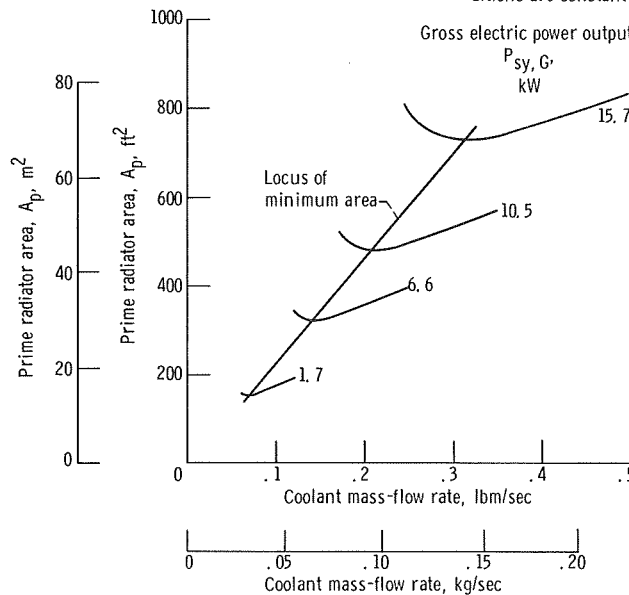
Figure 2(b) shows the required compressor-outlet pressure plotted against gross power output. For 2 kilowatts of output, a compressor-outlet pressure of 16.5 psia ($114 \text{ kN/m}^2 \text{ abs}$) was needed, while at 15.7 kilowatts, the required pressure increased to 61 psia ($421 \text{ kN/m}^2 \text{ abs}$). Over the range from about 2 to 10 kilowatts, required



(c) Changes in rotating-machinery and recuperator performance with gross power output.



(d-2) Inlet temperatures.
(d) Coolant mass-flow rates and temperatures that provide the design compressor-inlet temperature. Gas-loop conditions are constant for each value of gross power.



(e) Changes in radiator-area needs with coolant mass-flow rate and gross power. Gas-loop conditions are constant for each value of gross power output. Effective radiator heat-sink temperature, $450^\circ R$ ($250 K$).

Figure 2. - Concluded.

pressure was almost linear with power level.

Figure 2(c) shows the predicted rotating-machinery and recuperator operating conditions plotted against gross system power output. With increasing gross power, the required compressor pressure ratio decreased, while the turbine pressure ratio increased. Cycle-loss pressure ratio, used as a relative measure of total system pressure losses, increased from 0.895 at 2 kilowatts to 0.938 at 15.6 kilowatts. This trend resulted from the heat-exchanger and ducting pressure drops increasing at a lower rate than the gas pressure level itself. At 10 kilowatts, the cycle-loss pressure ratio is predicted to be 0.928, rather than the analytical design value of 0.92 (table I). This was a result of conservatism in assigning heat-exchanger and ducting design pressure drops.

Predicted recuperator heat-transfer effectiveness decreased from about 0.96 at 2 kilowatts to about 0.93 near 16 kilowatts. The recuperator heat-transfer coefficient increases with increasing gas mass-flow rate or power output. However, the amount of heat to be transferred over the fixed core surface area also increases. The net effect is a decrease in effectiveness with increasing power output. At 10 kilowatts, the recuperator effectiveness is about 0.94 (see appendix C) rather than the design value of 0.95 (table I).

Rotating-machinery efficiencies are also shown in figure 2(c). Both turbine and compressor efficiencies were based on total temperature and pressures. Since the turbine and compressor are small (ref. 2) and operate over a range of gas densities, viscous effects on their efficiencies were considered. Reynolds number corrections were made on the efficiencies obtained from turbomachinery maps to account for the viscous effects (appendix C and ref. 8). The increase in turbine and compressor efficiency (fig. 2(c)) with increasing output power were primarily due to the Reynolds number correction. The effect was much greater for the turbine than for the compressor. Over the power range in figure 2(c), turbine efficiency changed by about 0.04, while compressor efficiency changed by about 0.01.

At 10 kilowatts of gross system output, turbine efficiency was about 0.91 and compressor efficiency was 0.79. The compressor operating point with the design compressor-diffuser vane angle was below the peak compressor efficiency of 0.82.

Alternator electromagnetic efficiency had a peak value of about 0.91 at 6 kilowatts of gross system output. Inclusion of windage losses reduced the overall alternator efficiency. The peak overall alternator efficiency was 0.86 and occurred at about 7 kilowatts of gross system output. Alternator windage, although reduced in level, was a bigger part of the output at the lower power levels. This accounted for the increasing difference between electromagnetic and overall alternator efficiency with decreasing system output.

Figure 2(d) shows those combinations of coolant mass-flow rates and waste-heat-exchanger coolant temperatures that provide the design compressor-inlet temperature.

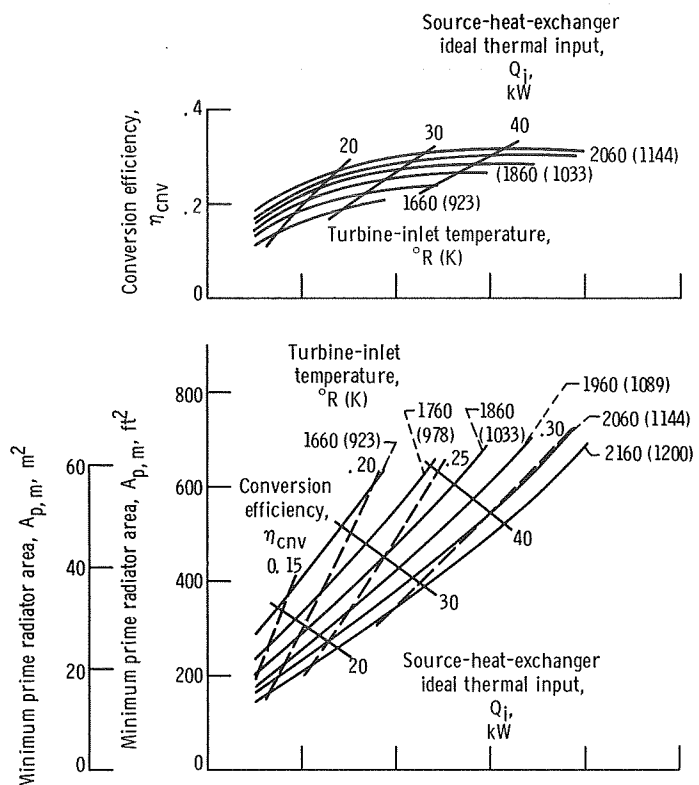
Matching curves are shown for four gross system output power levels. The power levels correspond to four values of constant gas inventory. For fixed gas-loop conditions, increasing coolant mass-flow rate resulted in increasing heat-transfer effectiveness. The coolant-inlet temperature rose asymptotically toward the fixed compressor-inlet temperature, while the resulting coolant-outlet temperature dropped because of the fixed heat load. As a result of these temperature changes, there was one value of coolant mass-flow rate for each output power level that resulted in a minimum prime radiator area. The heat rejected per unit of radiator surface area varies as the fourth power of the radiating temperature of that segment. Hence, there is a trade-off between decreasing radiator-inlet temperature and increasing radiator-outlet temperature.

Figure 2(e) shows the prime radiator area needs plotted against coolant mass-flow rate for the four values of gross output power. The locus of minimum prime area needs was approximately linear with coolant mass-flow rate. Lines are crossplotted on figure 2(d) to show the waste-heat-exchanger coolant temperatures associated with the locus of minimum-area mass-flow rates. On the basis of minimum specific prime radiator area, a ratio $A_{p, m}/P_{sy, G}$ of about 80 square feet per kilowatt ($7.4 \text{ m}^2/\text{kW}$) was needed at about the 2-kilowatt level, decreasing to about 46 square feet per kilowatt ($4.3 \text{ m}^2/\text{kW}$) in the range from 10 to 15 kilowatts. Due to simplifying assumptions in the calculation of radiator area (see pp. 33 and 55), the actual minimum area needs will be about 20 percent larger.

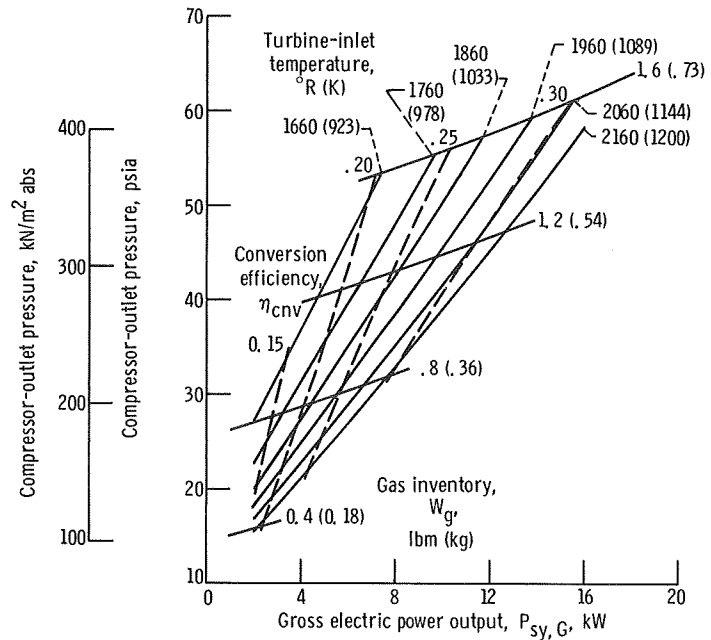
Turbine-inlet temperature effects. - Turbine-inlet temperature was studied over a range from 1660° to 2160° R (923 to 1200 K) in 100° R (56 K) changes. The lowest temperature was picked to determine conversion efficiency at zirconium-hydride-reactor temperature levels. The highest temperature, which exceeds the design value by 100° R (56 K), was examined to establish trends.

Figure 3 shows the effects of varying turbine-inlet temperature on system operation at design compressor-inlet temperature. Working-gas inventory was the independent variable. Figure 3(a) shows conversion efficiency and minimum prime radiator area needs plotted against power output. (In contrast to fig. 2(d), only the minimum areas are shown in fig. 3(a).) Lines of constant source-heat-exchanger ideal thermal input are shown, and lines of constant conversion efficiency are crossplotted on the radiator area curves. Figure 3(b) shows compressor-outlet pressure plotted against gross power output. Lines of constant gas inventory and conversion efficiency are crossplotted on the curves.

Trends in system operating conditions at each value of turbine-inlet temperature are similar to those at the design value. Maintaining constant gross system power output with decreasing turbine-inlet temperature requires increased source thermal input (fig. 3(a)) and increased gas inventory and compressor-outlet pressure (fig. 3(b)). The resulting conversion efficiency decreases, while the required minimum prime radiator



(a) Changes in efficiency and radiator area needs with gross power output and turbine-inlet temperature. Effective radiator heat-sink temperature, $450^{\circ}R$ (250 K).



(b) Changes in compressor-outlet pressure with gross power output and turbine-inlet temperature.

Figure 3. - Effects of turbine-inlet temperature on system operation at design compressor-inlet temperature. Working gas, helium-xenon (molecular weight, 83.8).

areas increase (fig. 3(a)). Maintaining constant source thermal input (fig. 3(a)) or gas inventory (fig. 3(b)) with decreasing turbine-inlet temperature results in decreasing system power output.

System operation at 2160° R (1200 K), if it is possible, would gain about 0.015 in conversion efficiency over that at the design inlet temperature. At a turbine-inlet temperature of 1660° R (923 K), the highest studied value of gas inventory (fig. 3(b), 1.6 lbm or 0.73 kg) resulted in a gross system power output of 7.5 kilowatts. Conversion efficiency at 1600° R increased from 0.11 at 2 kilowatts to about 0.21 at 7.5 kilowatts.

Compressor-inlet temperature effects. - Compressor-inlet temperature was studied over a range from 520° to 600° R (289 to 333 K) in 20° R (11 K) changes. The upper value was chosen to be typical of reactor-type system operation, while the lower value was used to establish potential conversion efficiency gains over those at the design inlet temperature.

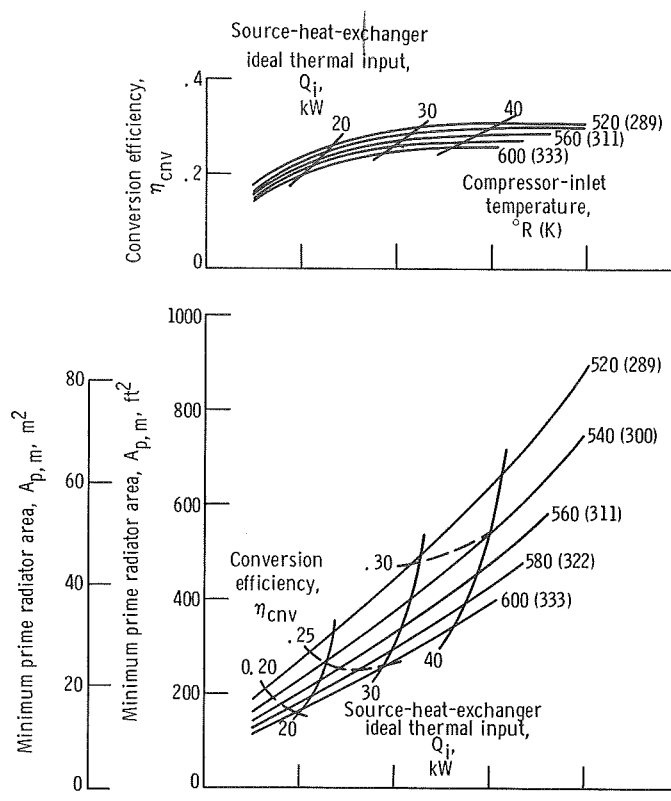
Figure 4 shows the effects of varying compressor-inlet temperature on system operation at design turbine-inlet temperature. The same format as in figure 3 was repeated in figure 4.

Trends in system operating conditions at each value of compressor-inlet temperature are similar to those at the design value. Maintaining constant power output with increasing compressor-inlet temperature requires increased source thermal input (fig. 4(a)) and increased gas inventory and compressor-outlet pressure (fig. 4(b)). The resulting conversion efficiency and required minimum prime radiator area both decrease (fig. 4(a)). Maintaining source thermal input (fig. 4(a)) or gas inventory (fig. 4(b)) constant with increasing compressor-inlet temperature results in decreasing system power output.

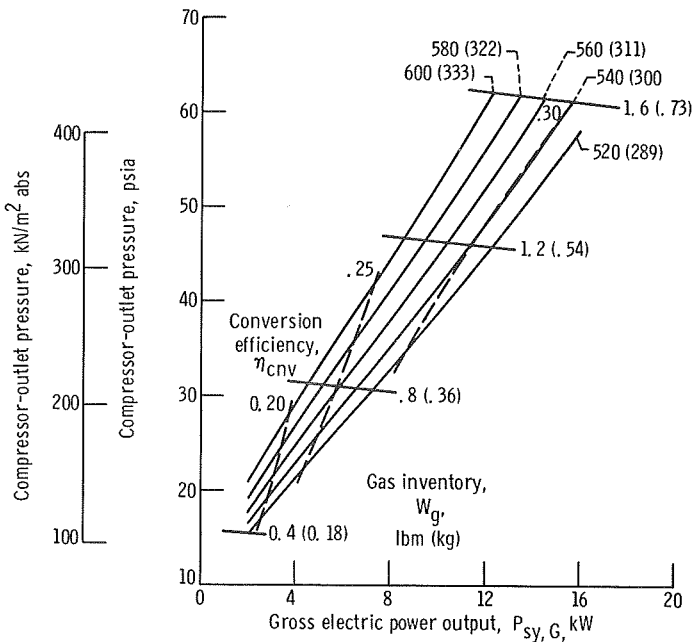
System operation at 520° R (289 K) would gain about 0.01 in conversion efficiency over that at the design inlet temperature; however, the required radiator area would increase. At a compressor-inlet temperature of 600° R (333 K), the highest studied value of gas inventory (fig. 4(b), 1.6 lbm or 0.73 kg) resulted in a gross system power output of 12.3 kilowatts. Conversion efficiency at 600° R increased from about 0.15 at 2 kilowatts to about 0.26 in the 9- to 12-kilowatt range.

Operation with krypton. - Krypton has a molecular weight of 83.8, and its viscosity is about the same as the design gas mixture. Therefore, the fluid-dynamic losses with either krypton or the design mixture are about the same. Krypton has a thermal conductivity lower than that of the mixture, which reduces heat transfer. Initial system tests will use krypton as the working gas since it is much less expensive.

Comparative system operation with krypton and the design mixture of helium and xenon is shown in figure 5 for the design turbine- and compressor-inlet temperatures. Conversion efficiency and minimum required prime radiator area are plotted against



(a) Changes in efficiency and radiator-area needs with gross power output and compressor-inlet temperature. Effective radiator heat-sink temperature, 450° R (250 K).



(b) Changes in compressor-outlet pressure with gross power output and compressor-inlet temperature.

Figure 4. - Effects of compressor-inlet temperature on system operation at design turbine-inlet temperature. Working gas, helium-xenon (molecular weight, 83.8).

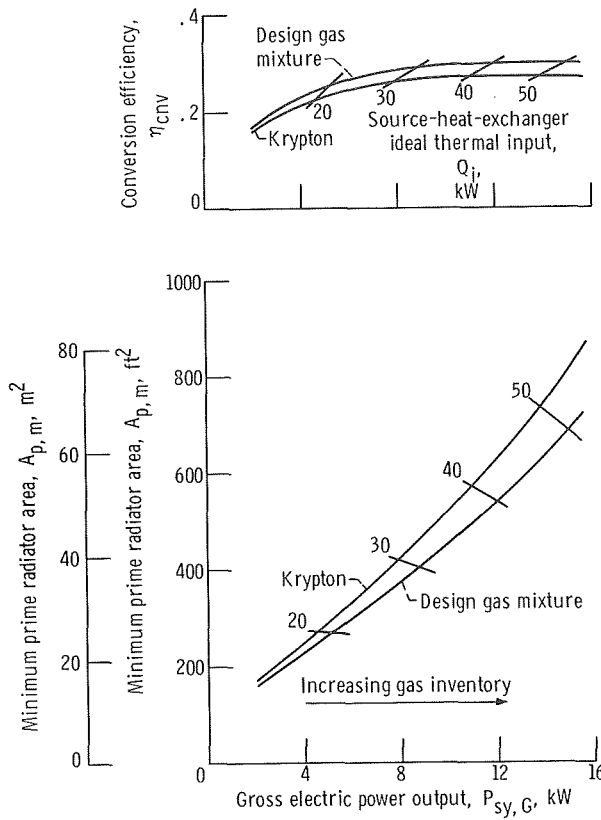


Figure 5. - Comparative system operation with krypton and design gas mixture. Turbine-inlet temperature, 2060° R (1144 K); compressor-inlet temperature, 540° R (300 K); effective radiator heat-sink temperature, 450° R (250 K).

gross system output power. Four lines of constant source ideal thermal input are cross-plotted on the results.

Due to the lower thermal conductivity of krypton, conversion efficiencies were lower, and minimum required prime radiator areas were larger, than those with the use of the gas mixture. More heat-source thermal input was needed to obtain the same output power obtained with the design mixture. The same compressor-outlet pressures were required for both the mixture and krypton at any value of gross output power. With the use of krypton, conversion efficiency increased from about 0.16 at 2 kilowatts of output to about 0.27 in the range from 10 to 16 kilowatts. Compared with the design gas mixture, conversion efficiency was lower by 0.01 at the 2-kilowatt level and by about 0.03 in the 10- to 16-kilowatt range.

Gas-mixture relative helium mass effects. - For the design molecular weight of 83.8, the helium mass is 1.78 percent of the total gas mass. The helium volume is 37.3 percent of the total gas volume. To determine the sensitivity of system conversion efficiency due to errors in gas mixing, the effects of ± 20 percent changes in the relative

helium mass were studied at the design turbine- and compressor-inlet temperatures.

At all system gross output power levels in the range from 2 to about 16 kilowatts, changes in conversion efficiency were small with the ± 20 percent change in relative helium mass. The largest changes occurred at about the 8-kilowatt output power level. There, the ± 20 percent mass change caused a ± 0.004 change in conversion efficiency. With increased helium mass content, the compressor-map operating point, although at a lower corrected speed, shifted more toward peak efficiency. Increasing helium mass content increased compressor efficiency and heat-transfer effectiveness, but decreased turbine efficiency.

Further increases in relative helium mass above 20 percent would result in additional small gains in conversion efficiency. At some point the trend would reverse. However, determining the relative helium mass increase needed to maximize conversion efficiency was beyond the purpose of this study. For errors in gas mixing as large as ± 20 percent of the relative helium mass, there would be little effect on system conversion efficiency.

Simulated Solar Operation

Calculations were made for simulated solar-power-system operation. Corresponding to the source configuration in reference 2, a solar-heat receiver designed for 40.5 kilowatts of average thermal input to the design gas mixture at a turbine-inlet temperature of 1960° R (1089 K) was assumed. Operation was assumed with a simulated prime radiator area of 500 square feet (46.5 m^2). An effective radiator heat-sink temperature of 400° R (222 K) was used. This sink temperature corresponds to a cylindrical radiating surface that is oriented parallel to the direction of the Sun and in a low Earth orbit (ref. 9). Since the solar collector must be oriented with respect to the Sun, the lower sink temperature for this case is reasonable.

The study was made to predict changes in conversion efficiency with changes in gas inventory for this type of ground-simulated, fixed-system operation. Turbine-inlet temperature was kept at 1960° R (1089 K) independent of gas inventory. In space, with a fixed solar-heat receiver, turbine-inlet temperature would change somewhat with gas inventory and orbital position.

For any fixed radiator area and design level of source thermal input, there is a particular value of coolant mass-flow rate that maximizes conversion efficiency and power output. This optimum coolant mass-flow rate also results in the lowest value of compressor-inlet temperature. For the calculations presented herein, the optimized coolant mass-flow rate was 0.25 pound mass per second (0.11 kg/sec).

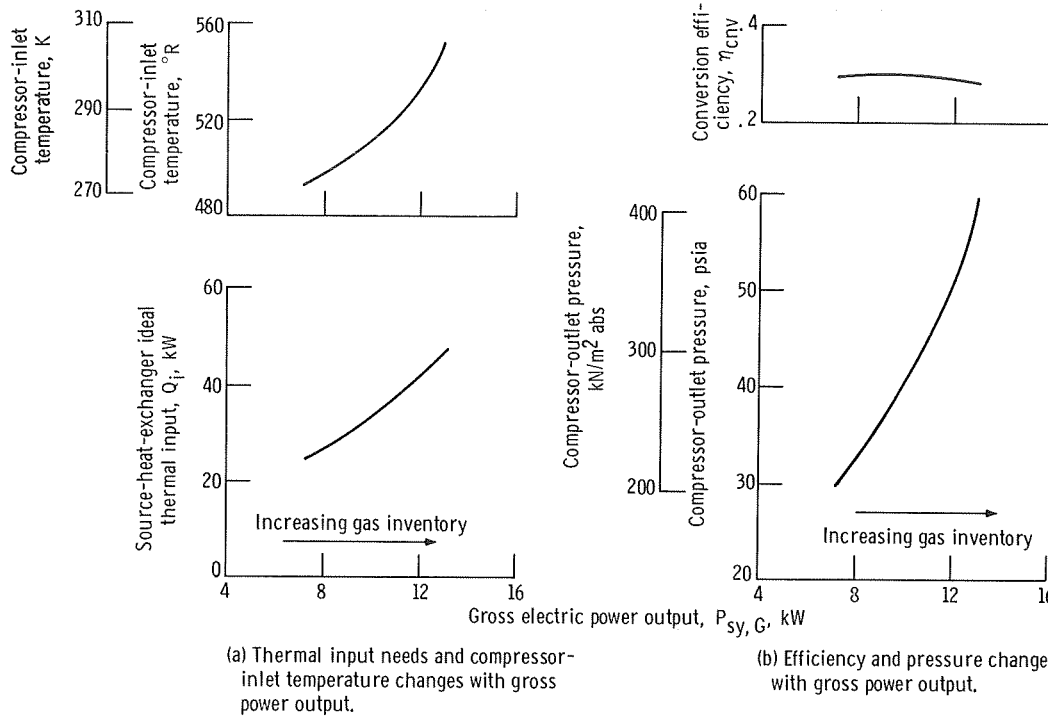


Figure 6. - Simulated solar operation. Turbine-inlet temperature, 1960° R (1089 K); working gas, helium-xenon (molecular weight, 83.8); effective radiator heat-sink temperature, 400° R (222 K); prime radiator area, 500 square feet (46.5 m^2); coolant mass-flow rate, 0.25 pound mass per second (0.11 kg/sec); design average thermal input, 40.5 kilowatts.

Figure 6 shows the changes in simulated solar-power-system operation due to changes in working-gas inventory. The optimized coolant mass-flow rate was used. Inventory was varied from 0.8 to 1.6 pounds mass in steps of 0.2 (0.36 to 0.73 kg in steps of 0.09). However, the results are plotted against gross system power output. Figure 6(a) shows the variations in compressor-inlet temperature and required source ideal thermal input, while figure 6(b) shows conversion efficiency and required compressor-outlet pressure.

The design average thermal input of 40.5 kilowatts resulted in 11.7 kilowatts of gross system power output. At 500 square feet of prime radiator area, 11.7 kilowatts of output was the maximum. The corresponding operating conditions were (1) compressor-inlet temperature, 526° R (292 K), (2) compressor-outlet pressure, 48.7 psia (336 kN/m^2 abs), and (3) conversion efficiency, 0.29.

For the simulated fixed-system operation, increasing gas inventory resulted in increasing power output. Compressor-inlet temperature, required source ideal thermal input, and compressor-outlet pressure all increased with increasing gas inventory. System conversion efficiency showed small changes with output power. At 7.1 kilowatts,

conversion efficiency was 0.292, while at 13.1 kilowatts it was 0.278. Conversion efficiency reached a peak value of 0.298 at 10 kilowatts.

For any fixed coolant mass-flow rate and radiator area, there are optimum values of source thermal input power and gas inventory that correspond with a peak in conversion efficiency. The value of input power at which peak efficiency occurs is primarily a function of the radiator area. The larger the radiator area, the higher the value of thermal input at peak efficiency. In figure 6(b), the difference between the conversion efficiency at 11.7 kilowatts and the peak efficiency at 10 kilowatts is small, about 0.01. A reoptimization in both coolant mass-flow rate and radiator area would result in only a small efficiency gain for the design average thermal input power level.

This calculation of simulated solar-power-system operation has shown that a space version with a design thermal power level and a limited amount of available radiator area should be optimized with coolant mass-flow rate to provide maximum power output. If radiator area is not limited, it could be chosen to prefer either design or off-design thermal input power operation; that is, a user could choose a large radiator area to maximize power output at design thermal input power, or he could pick a smaller area to keep a relatively high conversion efficiency over a range of lower-than-design input power.

Simulated Radioisotope Operation

Calculations were made for simulated radioisotope-power-system operation. Corresponding to the heat source in reference 2, a radioisotope source rated at 25 kilowatts thermal was studied. All of this thermal energy was assumed to radiate to the heat exchanger and be absorbed without loss by the system working gas. In a space version, both the radioisotope capsule array and adjacent source heat exchanger would be sized to provide the 25-kilowatt-thermal input to the gas at a turbine-inlet temperature of 2060° R (1144 K). Operation was assumed with a simulated prime radiator area of 350 square feet (32.5 m^2). An effective radiator heat-sink temperature of 450° R (250 K) was used. The coolant mass-flow rate, optimized for the assumed radiator area, the heat-source power level, and the design turbine-inlet temperature, was 0.155 pound mass per second (0.704 kg/sec). This value was held constant in the study.

The study was made to predict changes in conversion efficiency with changes in both working-gas inventory and radioisotope thermal power rating for the fixed-power-system operation. Since computed results give the required source ideal thermal input for an assigned turbine-inlet temperature, crossplotting was needed to obtain the results for constant values of source ideal thermal input.

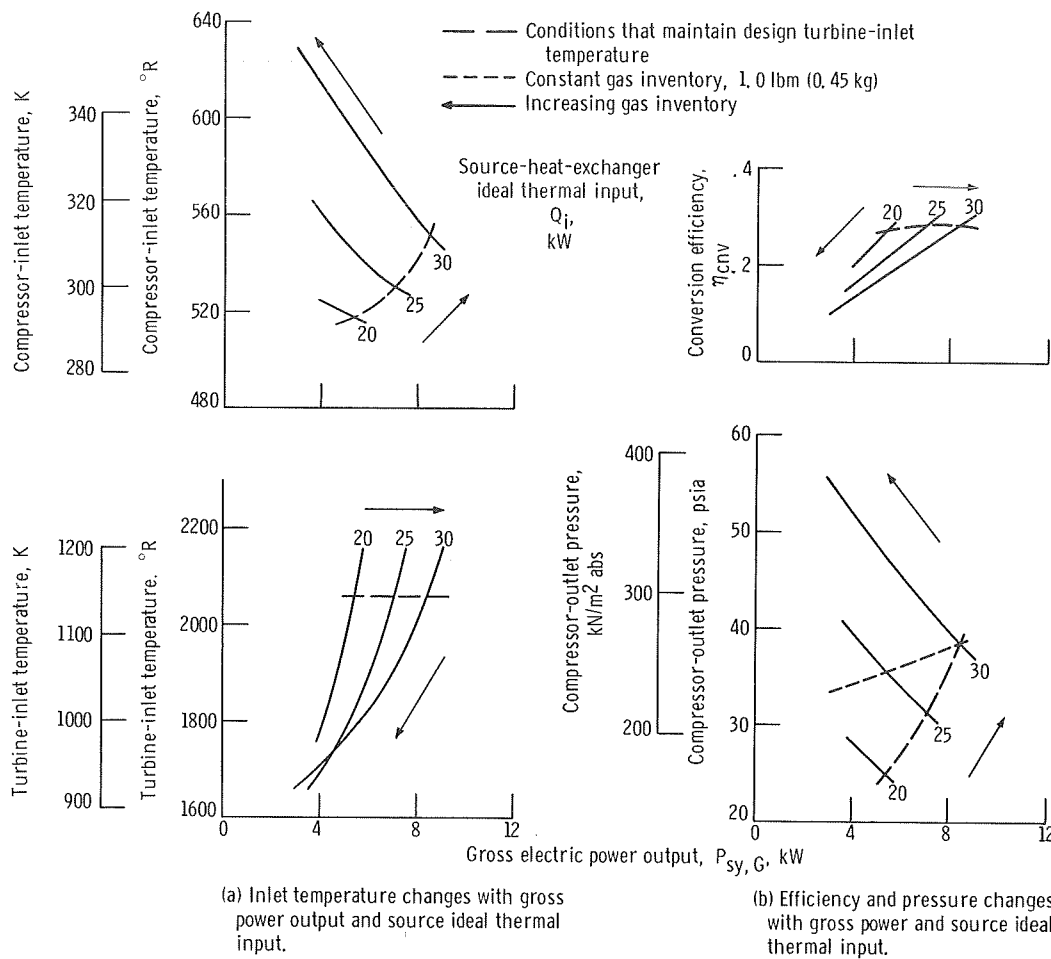


Figure 7. - Simulated radioisotope operation. Working gas, helium-xenon (molecular weight, 83.8); effective radiator heat-sink temperature, 450° R (250 K); prime radiator area, 350 square feet (32.5 m²); coolant mass-flow rate, 0.155 pound mass per second (0.794 kg/sec).

Figure 7 shows the changes in simulated, radioisotope-power-system operation due to changes in both working-gas inventory and source ideal thermal input power. The results for the assigned radiator conditions and the design gas mixture are plotted against gross system output power. Solid curves are used to present the results for three constant values of source-heat-exchanger ideal thermal input: 20, 25, and 30 kilowatts. Figure 7(a) shows the values of turbine- and compressor-inlet temperature. Figure 7(b) shows the values of conversion efficiency and compressor-outlet pressure.

Figure 7 shows that for a constant value of source thermal input power, an initially high value of gas inventory would result in the following relative operating conditions: high compressor-outlet pressure, low turbine-inlet temperature, high compressor-inlet temperature, and low conversion efficiency. Bleeding gas from the system would then improve operation.

At design turbine-inlet temperature with an ideal 25-kilowatt, source thermal input, the compressor-outlet pressure was 31.3 psia (216 kN/m^2 abs). The corresponding compressor-inlet temperature was 530° R (284 K), gross power output was about 7 kilowatts, and conversion efficiency was about 0.28.

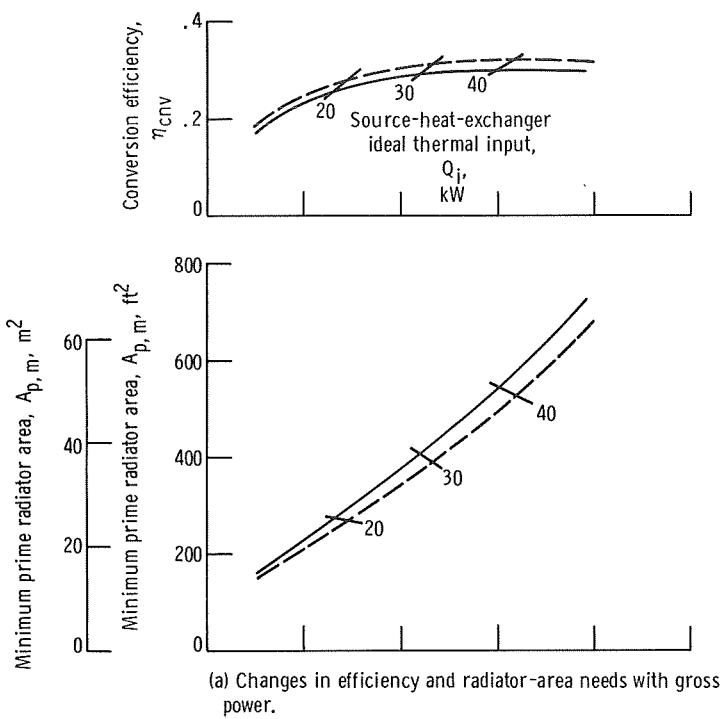
Figure 7(b) shows that, at the design turbine-inlet temperature conditions, a maximum conversion efficiency occurred for about 25 kilowatts of ideal thermal input. As was the case for simulated solar-power-system operation, with fixed values of radiator area and coolant mass-flow rate, there were particular values of source input and gas inventory that maximized power output for operation at the design turbine-inlet temperature.

The turbine-inlet-temperature curves (fig. 7(a)) for 25 and 30 kilowatts of thermal input intersect at about 4.6 kilowatts of output. For constant, but lower-than-design, turbine-inlet temperatures, the same fixed radiator conditions also result in unique maximum power output conditions. At reduced turbine-inlet temperatures, both the output power level and the value of source thermal input for maximum conversion efficiency operation are reduced. At a turbine-inlet temperature of 1740° R (966 K), the change in conditions for maximum power output was enough that increasing source input above 25 kilowatts did not result in more output power.

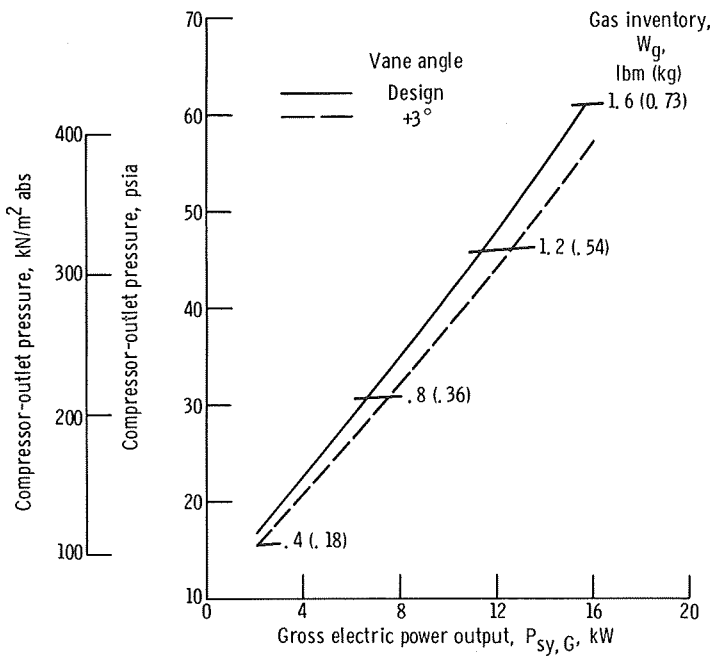
The constant-design-turbine-inlet-temperature curves (long-dashed curves) of figure 7 also show a way in which power output could be controlled during decay of a short-lived radioisotope. If a source was rated for 30 kilowatts input at the "start of mission," the system could initially produce about 8.5 kilowatts of gross power at the rated turbine-inlet temperature. Conversion efficiency, about 0.28, would be only slightly below its peak value. As the source decays, and if no change is made to the system operation, its power output would drop as indicated by the constant-gas-inventory line (short-dashed curve) in figure 7(b). After decay to 25 kilowatts (a 16.7 percent decrease), the gross output power would drop to about 5.5 kilowatts (or a 36 percent decrease). However, if the working gas is bled off (reducing system pressure level) to maintain the design turbine-inlet temperature during source decay from 30 to 25 kilowatts, gross power output would drop to 7.1 kilowatts, or only 16 percent. From the upper curves in figure 7(b), such operation would maintain a relatively high conversion efficiency over a 33 percent decay from the initial 30 kilowatts.

Reset Compressor-Diffuser Vanes

Up to this section all results were based on the present hardware intended for use in the system ground tests. The design compressor-diffuser vane angle was chosen to provide margin from compressor surge as protection in case of mismatched system op-



(a) Changes in efficiency and radiator-area needs with gross power.



(b) Changes in gas pressure and inventory with gross power.

Figure 8. - System performance gains with $+3^\circ$ compressor diffuser. Design inlet temperatures and design gas mixture.

erating conditions. This choice resulted in a compressor-corrected mass-flow rate, at system design conditions, above that corresponding to peak compressor efficiency. Results of unpublished tests on this compressor at Lewis, over a range in vane angles, have shown that a 3° increase would result in a shift to peak compressor efficiency for design system operation.

This analysis has shown no mismatch in system operating conditions. Hence, if this is confirmed in the system ground tests, the use of a modified, $+3^{\circ}$ compressor-diffuser would be desirable.

Figure 8 shows the potential system operational gains with the use of a $+3^{\circ}$ compressor-diffuser. Results are shown for both the design and modified compressor-diffuser at the design turbine- and compressor-inlet temperatures plotted against gross system output power. The design gas mixture was used and the range in gas inventory from 0.4 to 1.6 pounds mass (0.18 to 0.73 kg) was studied. Figure 8(a) shows conversion efficiency and minimum required prime radiator area, while figure 8(b) shows the required compressor-outlet pressures. Four lines of constant source ideal thermal input are crossplotted on the results in figure 8(a). The four lines of constant gas inventory are shown in figure 8(b).

With the modified compressor-diffuser, conversion efficiency increased from about 0.18 at 2 kilowatts of output to about 0.32 in the 10- to 15-kilowatt power range. Over the 2- to 15-kilowatt output range, the gain in conversion efficiency with the modified compressor was between 0.01 and 0.02. The gains in conversion efficiency were primarily due to increased compressor efficiency. At the 10-kilowatt level with the $+3^{\circ}$ diffuser, compressor efficiency was at its peak value of about 0.83. (The modified diffuser increased the peak compressor efficiency by about 0.01 over that of the design diffuser, see p. 12).

More power output for the same thermal power input was obtained with the use of the modified diffuser. Over the power output range, use of the $+3^{\circ}$ diffuser reduced the minimum required specific prime radiator area by between 4 and 5 square feet per kilowatt (0.4 and $0.5 \text{ m}^2/\text{kW}$). Figure 8(b) shows that, for the same output power, the use of the modified diffuser resulted in lower required compressor-outlet pressure and gas inventory.

CONCLUDING REMARKS

This analysis approximated the power system configuration being ground tested. Because some real-system effects were neglected (see p. 7), the computed levels of system conversion efficiency must be considered ideal. However, the trends of the results should be correct.

The neglected effects may lower the level of system conversion efficiency shown in the analysis by about 20 percent. Therefore, before experimental results are available, system conversion efficiency at design conditions should be considered to be about 0.14 at 2 kilowatts of output, increasing to about 0.24 in the 10- to 15-kilowatt range. All other trends shown in the analytical results should be referenced to this reduced efficiency level.

SUMMARY OF RESULTS

A steady-state digital-computer study of a Brayton power system was made to examine parametric and simulated-fixed-system operations to be conducted in experimental system ground tests. The analysis shows trends in conversion efficiency and is independent of present system operational limits. However, the present limitations of the existing hardware are discussed.

Unless noted otherwise, the results are summarized for the design working gas, a mixture of helium and xenon at a molecular weight of 83.8; the design turbine-inlet temperature, 2060° R (1144 K); and the design compressor-inlet temperature, 540° R (300 K). Major study results were as follows:

1. Estimated levels of system conversion efficiency, including an allowance for losses neglected in the analysis, increased from about 0.14 at 2 kilowatts of output to about 0.24 in the 10- to 15-kilowatt range. The ideal, predicted levels were 0.17 at 2 kilowatts and 0.30 in the 10- to 15-kilowatt range.
2. Future power system gains were predicted with the use of a compressor-diffuser modified by a 3° increase in vane angle. With the modified diffuser, the analysis showed potential conversion efficiency gains of 0.01 at the 2-kilowatt output power level, and of 0.02 in the 10- to 15-kilowatt range.
3. Calculations for both simulated solar- and radioisotope-power-system operation showed that with fixed values of space radiator area and coolant mass-flow rate, there were particular values of source thermal input power and gas inventory that maximized gross system power output.
4. Simulated radioisotope-power-system calculations showed that bleeding working gas would be an effective means to maintain high system electric power output during the decay of a short-lived radioisotope.
5. Calculations showed that, with the use of krypton as the system working gas, conversion efficiency would decrease by about 0.01 at 2 kilowatts of output and by about 0.03 in the 10- to 15-kilowatt range.

6. A ± 20 percent change in the relative helium mass of the working-gas mixture caused no more than a ± 0.004 change in conversion efficiency within the 2- to 15-kilowatt output power range.

Lewis Research Center,

National Aeronautics and Space Administration,

Cleveland, Ohio, September 25, 1969,

120-27.

APPENDIX A

SYMBOLS

A	heat-transfer surface area, ft^2 ; m^2
A_p	ideal prime space radiator area (see p. 33 and eq. (C103)), ft^2 ; m^2
C_w	waste-heat-exchanger capacity-rate ratio, $mc_p / (mc_p)_l$
C_1	constant defined in eq. (C9), $(^0\text{R})(\text{lbm}) / (\text{ft})(\text{lbf})(\text{rpm})$; $(\text{K})(\text{kg}) / (\text{N})(\text{m})$
C_2	constant defined in eq. (C21), dimensionless
c_p	specific heat at constant pressure, $\text{Btu}/(\text{lbm})(^0\text{R})$; $\text{J}/(\text{kg})(\text{K})$
D_t	tip diameter, ft ; m
E	heat-transfer effectiveness
f	friction coefficient
f', g', h'	functions of ()
f_{cw}	compressor work factor, $\frac{(60)^2 g J c_p (T_5 - T_4)}{\pi^2 N^2 D_{t, C}^2}, \text{ dimensionless};$ $\frac{g c_p (T_5 - T_4)}{\pi^2 N^2 D_{t, C}^2} \times 10^4$
G	mass-flow rate per unit area, $\text{lbm}/(\text{ft}^2)(\text{sec})$; $\text{kg}/(\text{m}^2)(\text{sec})$
g	acceleration due to gravity, $32.2 \text{ (ft)(lbm)}/(\text{sec}^2)(\text{lbf})$; $9.81 \text{ (m)(kg)}/(\text{sec}^2)(\text{N})$
h	local heat-transfer coefficient, $\text{Btu}/(\text{sec})(\text{ft}^2)(^0\text{R})$; $\text{J}/(\text{sec})(\text{m}^2)(\text{K})$
i	a number index
J	mechanical equivalent of heat, $778 \text{ (ft)(lbf)}/\text{Btu}$; $1 \text{ (m)(N)}/\text{J}$
j	Colburn factor for heat transfer, $(h/Gc_p)(Pr)^{2/3}$, dimensionless
K	molecular weight correction factor, $83.8/M_w$
K_{eq}	equivalent duct length-to-diameter ratio (eq. (C94)), dimensionless
k	thermal conductivity, $\text{Btu}/(\text{sec})(\text{ft})(^0\text{R})$; $\text{J}/(\text{sec})(\text{m})(\text{K})$
L_b	bearing friction loss, kW
L_w	alternator windage loss, kW

M_w molecular weight

m mass-flow rate, lbm/sec; kg/sec

N shaft rotational speed, rpm; rad/sec

$N_{s, C}$ compressor specific speed,
$$\frac{\pi N \sqrt{\frac{m}{\rho_4}}}{1800 \left[g c_p T_4 \left(r_C^{(\gamma-1)/\gamma} - 1 \right) \right]^{3/4}}$$
, dimensionless;

N_{tu} number of thermal units, $UA / (mc_p)_m$, dimensionless

$$\frac{N \sqrt{\frac{m}{\rho_4}}}{\left[g c_p T_4 \left(r_C^{(\gamma-1)/\gamma} - 1 \right) \right]^{3/4}}$$

n empirical exponent

n_p number of passes

P power, kW

P_e internal system electric power needs, kW

Pr Prandtl number, $\mu c_p / k$, dimensionless

$P_{sy, G}$ gross system electric power output (fig. 1), kW

p total gas pressure, psia; kN/m^2 abs

Q thermal power, kW

Q_i ideal thermal power input to gas in the heat-source heat exchanger, kW

Re Reynolds number, $\rho v D_t / \mu$, dimensionless

r_C compressor total-pressure ratio, p_5 / p_4

r_T turbine total-pressure ratio, p_1 / p_2

r_T / r_C cycle-loss pressure ratio

T total temperature, ${}^{\circ}\text{R}$; K

T_S effective radiator heat-sink temperature, ${}^{\circ}\text{R}$; K

U overall heat-transfer coefficient, $\text{Btu}/(\text{sec})(\text{ft}^2)({}^{\circ}\text{R})$; $\text{J}/(\text{sec})(\text{m}^2)(\text{K})$

V volume, ft^3 ; m^3

v velocity, ft/sec; m/sec

W_g	gas inventory, lbm; kg
Γ	mathematical function defined in eq. (C78)
γ	ratio of specific heats for a monatomic ideal gas, 5/3
Δ	difference operator
δ	ratio of compressor-inlet pressure to U. S. standard pressure, $p_4/14.69$ psi; $p_4/101.325$ kN/m ²
ϵ	radiator surface hemispherical emittance, 0.90
ζ	mathematical function defined in eq. (C80)
η	efficiency
η_{cnv}	conversion efficiency, $P_{sy,G}/Q_i$
η_{cy}	cycle efficiency, $P_{sh,G}/Q_i$
θ	ratio of compressor-inlet temperature to U. S. standard temperature, $T_4/519$ °R; $T_4/288$ K
μ	viscosity, lbm/(ft)(sec); kg/(m)(sec)
ρ	density, lbm/ft ³ ; kg/m ³
σ	Stefan-Boltzmann constant, 0.481×10^{-12} Btu/(sec)(ft ²)(°R ⁴); 5.73×10^{-8} J/(sec)(m ²)(K ⁴)
τ	turbine torque, ft/lbf; m/N
φ	waste-heat-exchanger performance factor defined in eq. (C76)

Subscripts:

a	alternator
C	compressor
c	cold side of recuperator
cs	compressor surge
em	electromagnetic
f	fin
G	gross
g	gas
h	hot side of recuperator
i	inlet

<i>l</i>	liquid
<i>m</i>	minimum
<i>n</i>	net
<i>o</i>	outlet
<i>P</i>	coolant pump
<i>p</i>	per pass
<i>R</i>	radiator
<i>r</i>	recuperator
<i>s</i>	surface
<i>sh</i>	shaft
<i>so</i>	source heat exchanger
<i>T</i>	turbine
<i>w</i>	waste heat exchanger
<i>1</i>	turbine-inlet station
<i>2</i>	turbine-outlet station
<i>3</i>	waste-heat-exchanger, gas-side, inlet station
<i>4</i>	compressor-inlet station
<i>5</i>	compressor-outlet station
<i>6</i>	source-heat-exchanger inlet station

Superscripts:

*	design or reference condition
—	average value
''	new value

APPENDIX B

DETAILS OF COMPUTER PROCEDURES

Fluid Properties

Values of gas viscosity and thermal conductivity were tabulated as functions of temperature and entered into the computer program as input data. These properties were obtained from Vanco's analysis (ref. 10). Pressure effects on the properties were small for the range of interest and were neglected. In the computer program, all tabular interpolations used Newton's formulas (ref. 11, pp. 61-66).

Coolant specific-heat values used in the liquid-loop calculations were obtained from testing three sample batches of the coolant over the temperature range from 77° to 300° F (298 to 422 K). The following linear fit was found and used in the program:

$$\left. \begin{aligned} c_{p,l} &= 3.10 T_l \times 10^{-4} + 0.239 \\ c_{p,l} &= 2.34 T_l + 1000 \end{aligned} \right\} \quad (B1)$$

(Where two equations are given, the first is in U. S. customary units and the second in SI units.)

Flow-Logic Diagrams

Flow-logic diagrams for the computer calculations are shown in figures 9 and 10. Figure 9 shows the logic paths for gas-loop closure which is common to both types of calculations in figure 10. Figure 10(a) shows the logic paths for the calculation of system parametric operation. And figure 10(b) shows the logic paths for simulated-fixed-system-operation calculations.

Gas-loop closure. - For either calculation, this part of the computer program is entered with assigned values for W_g , M_w , N , T_1 , and T_4 . Values are assumed for m and p_1 . During the first pass ($n_p = 1$) through this calculation, all ratio terms for heat-exchanger pressure drops and recuperator effectiveness, other than $(m/m^*)^n$, are set equal to 1. The logic requires more than one pass for each new entry. After the first pass, turbine-inlet temperature is lowered because of the seal loss model, and p_1 is corrected by $-(p_1'' - p_1)/2$.

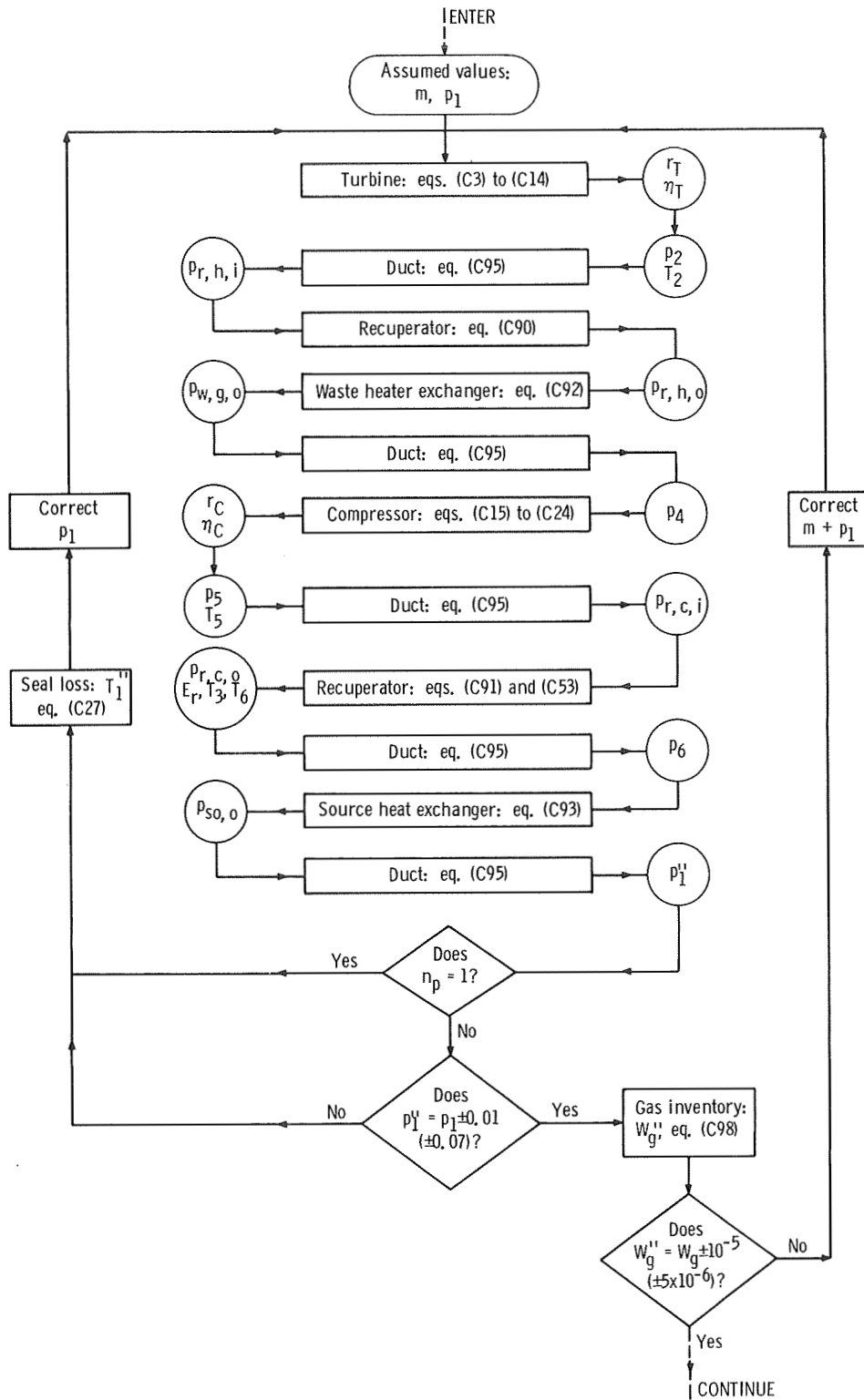
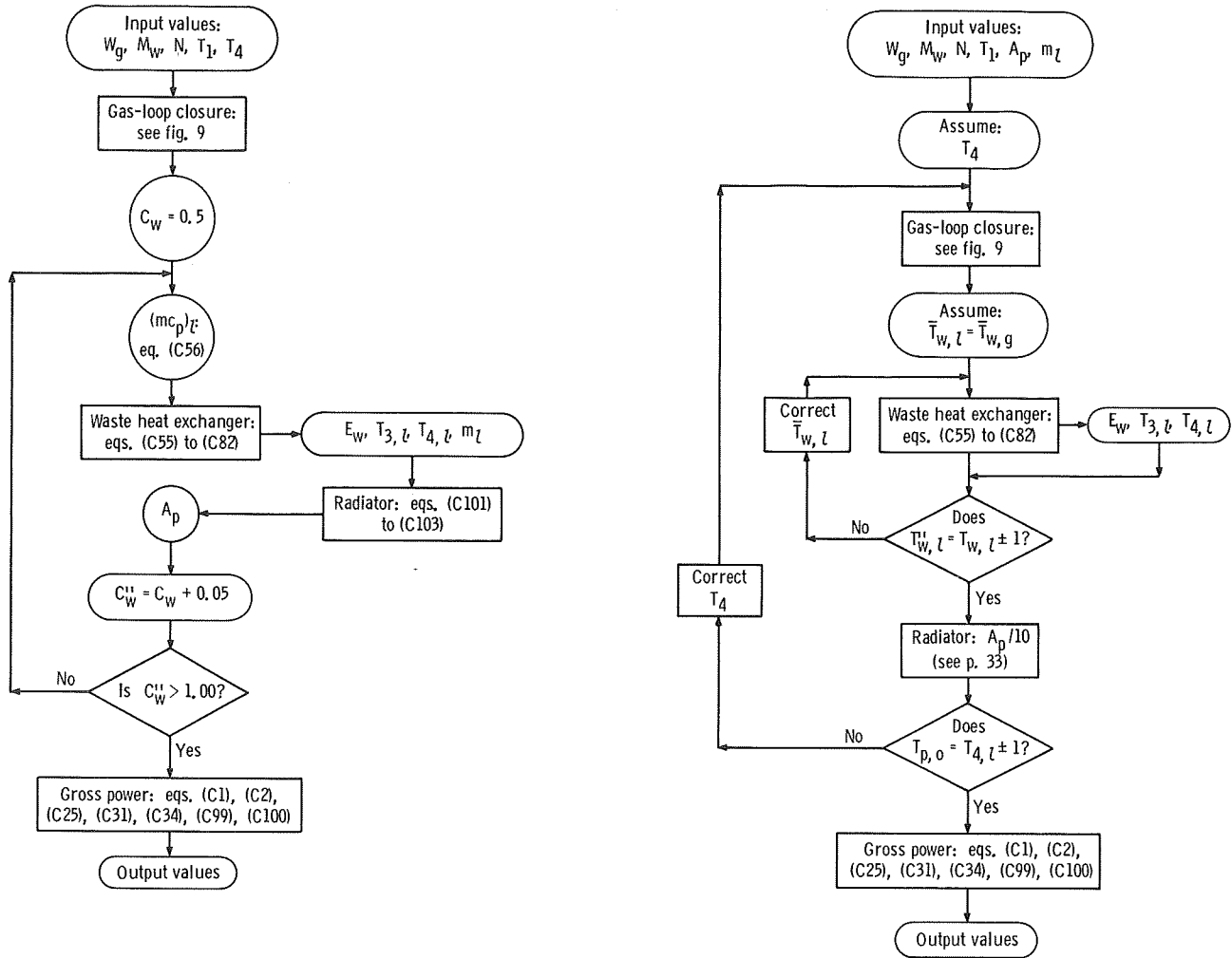


Figure 9. - Flow-logic diagram for gas-loop closure.



(a) Calculation of system parametric operation.

(b) Calculation of simulated fixed-system operation.

Figure 10. - Flow-logic diagrams for calculation of system operation.

The first iteration to be satisfied is that shown for turbine-inlet pressure p_1 . The second iteration, in series, is on working-gas inventory. Calculated inventory W_g'' is compared to the assigned value W_g in the problem input. If gas inventory is not satisfied, both m and p_1 are corrected and the process repeats. The changes are made based on linear variations of m and p_1 with W_g . Both m and p_1 are corrected for $-(W_g'' - W_g)/2$ times the respective linear ratio.

When both p_1 and W_g are satisfied, this part of the calculation is finished and the calculations shown in figure 10 continue.

Parametric system operation. - Input values (fig. 10(a)) for this calculation include W_g , M_w , N , T_1 , and T_4 . After the gas-loop calculations are satisfied, the waste-heat-exchanger capacity-rate ratio C_w is varied over a range of values from 0.5 to 1.0 in steps of 0.05. The liquid mass-flow rate is calculated from the liquid capacity rate $(mc_p)_l$ by evaluating $c_{p,l}$ from equations (B1) at $\bar{T}_{w,l}$ and dividing. After the range in C_w is complete, the remaining calculations for gross electric power output $P_{sy,G}$ are made, and the results are printed out.

Simulated fixed-system operation. - This type of calculation (fig. 10(b)) is a variation on the previous methods (fig. 10(a)). Here, A_p and m_l are assigned in place of T_4 in the input values. Initially, an arbitrary value of T_4 is assumed, and the gas-loop closure calculations are made. The waste-heat-exchanger calculations are made with an iteration on the temperature at which $c_{p,l}$ is evaluated.

The assigned prime radiator area is divided into 10-square-foot (0.93-m^2) sections. Each section is assumed to be isothermal and to reject heat radiantly at its liquid-inlet temperature. Hence, the calculation is approximate. It neglects the temperature drops across the section and between the coolant and the radiating surface. The inlet temperature to the first radiator section is $T_{3,l}$. Then, in sequence, the outlet temperature of each section is calculated from a heat balance, and is the inlet temperature for the next radiator section. The process ends when the outlet temperature of the last section $T_{R,o}$ is obtained. The coolant pump outlet temperature results from (see eq. (C102)).

$$\left. \begin{array}{l} T_{P,o} = T_{R,o} + 2 \\ T_{P,o} = T_{R,o} + 1 \end{array} \right\} \quad (B2)$$

If the liquid-loop temperatures $T_{P,o}$ and $T_{4,l}$ are not satisfied, the wrong T_4 was used. Then, T_4 is corrected by $(T_{4,l} - T_{P,o})/2$ and the calculation repeats. After satisfying both the gas- and liquid-loop temperatures, the remaining calculations for gross output power are made, and the results are printed out.

APPENDIX C

COMPONENT MODELS

Rotating Machinery

Gross shaft power $P_{sh,G}$ was defined as the difference between turbine work and compressor work. The net shaft power was then

$$P_{sh,n} = P_{sh,G} - L_b - L_w \quad (C1)$$

and the gross alternator power was

$$P_{a,G} = \eta_{em} P_{sh,n} \quad (C2)$$

Turbine. - The turbine performance maps were obtained from Nusbaum and Kofskey's results (ref. 3). Tables entered into the computer program were of the form

$$r_T = f\left(\frac{N}{\sqrt{T_1}}, \frac{m\sqrt{T_1}}{p_1}\right) \quad (C3)$$

and

$$\frac{\tau}{p_1} = g\left(\frac{N}{\sqrt{T_1}}, r_T\right) \quad (C4)$$

For each turbine calculation, the tables were entered with known values of $N/\sqrt{KT_1}$ and $m\sqrt{KT_1}/p_1$. A double interpolation, using Newton's formulas, calculated r_T for these values. Then another double interpolation solved for τ/p_1 .

Monatomic perfect-gas relations were assumed, thus

$$\gamma = \frac{5}{3} \quad (C5)$$

and

$$\left. \begin{aligned} c_p &= \frac{\gamma}{\gamma - 1} \left(\frac{1545}{JM_w} \right) \\ c_p &= \frac{\gamma}{\gamma - 1} \left(\frac{8322}{M_w} \right) \end{aligned} \right\} \quad (C6)$$

Turbine efficiency resulted from

$$\eta_T = \frac{C_1 \left(\frac{\tau N}{m K T_1} \right)}{1 - r_T^{-(\gamma-1)/\gamma}} \quad (C7)$$

where

$$\frac{\tau N}{m K T_1} = \frac{\left(\frac{\tau}{p_1} \right) \left(\frac{N}{\sqrt{K T_1}} \right)}{\frac{m \sqrt{K T_1}}{p_1}} \quad (C8)$$

and

$$\left. \begin{aligned} C_1 &\equiv \frac{\pi}{30 J c_p^*} = 2.27 \times 10^{-3} \\ C_1 &\equiv \frac{1}{c_p^*} = 4.02 \times 10^{-3} \end{aligned} \right\} \quad (C9)$$

with c_p^* given by equations (C6) evaluated for $M_w = 83.8$. A Reynolds number correction for efficiency was assumed, using the general form (see Shepherd, ref. 8)

$$\Delta(\eta) = (1 - \eta^*) \left[1 - \left(\frac{Re^*}{Re} \right)^n \right] \quad (C10)$$

Nusbaum and Kofskey's results were used to adapt equation (C10) for use with the turbine maps. Turbine Reynolds number was defined as

$$Re_T'' \equiv \frac{2m}{\mu_1 D_{t,T}} \quad (C11)$$

This number is related to the conventional usage by

$$Re_T'' = \frac{2}{\pi} Re_T \quad (C12)$$

The resulting correction was

$$\Delta(\eta_T) = 0.112 \left[1 - \left(\frac{7.62 \times 10^4}{Re_T''} \right)^{0.25} \right] \quad (C13)$$

such that

$$\eta_T'' = \eta_T + \Delta(\eta_T) \quad (C14)$$

Compressor. - The compressor experimental performance results have not been published. Figure 11, however, is a sketch of the compressor map formats that were used. A transformation was made before entering tabular values into the computer program for ease of interpolation with Newton's formulas. All compressor input data were

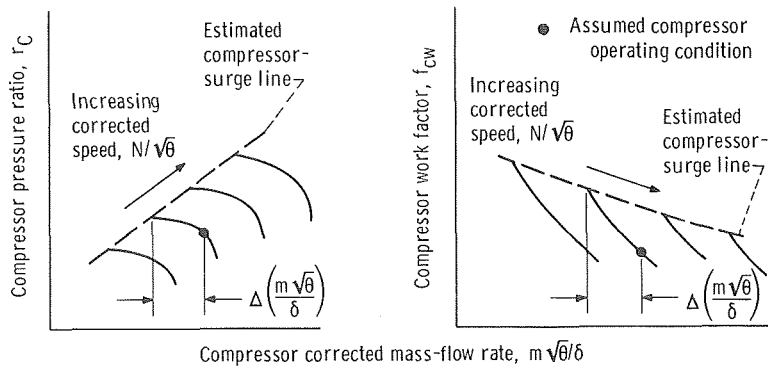


Figure 11. - Experimental compressor maps.

referenced to the estimated compressor surge lines, shown dashed in figure 11. The computer tables were of the form

$$\left(\frac{m \sqrt{\theta}}{\delta} \right)_{cs} = f' \left[\begin{array}{l} \frac{N}{\sqrt{\theta}} \\ \frac{\sqrt{\theta}}{\left(\frac{N}{\sqrt{\theta}} \right)^*} \\ \left(\frac{N}{\sqrt{\theta}} \right)^* \end{array} \right] \quad (C15)$$

$$r_C = g' \left[\begin{array}{l} \frac{N}{\sqrt{\theta}} \\ \frac{\sqrt{\theta}}{\left(\frac{N}{\sqrt{\theta}} \right)^*}, \Delta \left(\frac{m \sqrt{\theta}}{\delta} \right) \\ \left(\frac{N}{\sqrt{\theta}} \right)^* \end{array} \right] \quad (C16)$$

$$f_{cw} = h' \left[\begin{array}{l} \frac{N}{\sqrt{\theta}} \\ \frac{\sqrt{\theta}}{\left(\frac{N}{\sqrt{\theta}} \right)^*}, \Delta \left(\frac{m \sqrt{\theta}}{\delta} \right) \\ \left(\frac{N}{\sqrt{\theta}} \right)^* \end{array} \right] \quad (C17)$$

where

$$\Delta \left(\frac{m \sqrt{\theta}}{\delta} \right) = \left(\frac{m \sqrt{\theta}}{\delta} \right) - \left(\frac{m \sqrt{\theta}}{\delta} \right)_{cs} \quad (C18)$$

and

$$\left. \begin{array}{l} \left(\frac{N}{\sqrt{\theta}} \right)^* = 35300 \\ \left(\frac{N}{\sqrt{\theta}} \right)^* = 3700 \end{array} \right\} \quad (C19)$$

For each compressor calculation, the tables were entered with known values of $N/\sqrt{K\theta}$ and $m\sqrt{K\theta}/\delta$. A single interpolation and equation (C18) resulted in $\Delta(m\sqrt{\theta}/\delta)$. Two double interpolations gave values for r_C and f_{cw} .

Compressor efficiency resulted from

$$\eta_C = \frac{r_C^{(\gamma-1)/\gamma} - 1}{C_2 \left[\left(\frac{N}{\sqrt{K\theta}} \right)^2 + f_{cw} \left(\frac{N}{\sqrt{\theta}} \right)^* \right]} \quad (C20)$$

where

$$\left. \begin{aligned} C_2 &\equiv \frac{\pi^2 D_{t,C}^2 \left(\frac{N}{\sqrt{\theta}} \right)^*}{519(25) g J c_p^*} = 0.556 \\ C_2 &\equiv \frac{D_{t,C}^2 \left(\frac{N}{\sqrt{\theta}} \right)^*}{288 g c_p^*} \end{aligned} \right\} \quad (C21)$$

with c_p^* given by equations (C6) evaluated for $M_w = 83.8$. The same Reynolds number correction form (eq. (C10)) was used for the compressor. And, similar to the definition for turbine Reynolds number, compressor Reynolds number was defined as

$$Re_C'' \equiv \frac{2m}{\mu_4 D_{t,C}} \quad (C22)$$

Based on the unpublished compressor performance results, the Reynolds number correction was

$$\Delta(\eta_C) = 0.207 \left[1 - \left(\frac{4.14 \times 10^5}{Re_C''} \right)^{0.06} \right] \quad (C23)$$

such that

$$\eta_C'' = \eta_C + \Delta(\eta_C) \quad (C24)$$

Alternator. - The alternator electromagnetic efficiency was obtained from Repas and Edkin's results (ref. 4). They show this efficiency plotted against gross alternator power $P_{a, G}$ for power factors of 0.75 and 1.0. Although a power factor higher than 0.75 may be expected in most uses, the 0.75 results were used here for conservatism. Electromagnetic efficiency was plotted, with use of equation (C2), against net shaft power $P_{sh, n}$ and extrapolated from 15 to 24 kilowatts. This extension was needed to examine operation near 16 kilowatts of gross power $P_{sy, G}$. The efficiency values were tabulated and entered into the computer program in the form

$$\eta_{a, em} = f'(P_{sh, n}) \quad (C25)$$

Seal losses. - Based on the analytical design of the rotating machinery, 2 percent of the compressor-outlet flow must be bled off to supply pressure to the gas bearings. The bleed flow is ducted from the compressor scroll into the bearing and shaft cavities. One-half of this flow is estimated to leak through the turbine-end, labyrinth shaft seal. This flow reenters the main flow just upstream of the turbine impeller. The other half of the bleed flow leaks through the compressor-end seal. It reenters the main flow just downstream of the compressor impeller and ahead of the diffuser vanes. The bleed flow is at or near the compressor-outlet total pressure. There is a sufficient pressure difference for the flow to reenter the main stream at the compressor-impeller exit, since there the flow is controlled by the local static pressure.

The leakage flow into the turbine causes a mixing loss. The leakage flow circulating around the compressor vanes causes an increased pumping loss. In the computer program, a difference in gas mass-flow rate was calculated as

$$m_c = \frac{0.98}{0.99} m_h \quad (C26)$$

where m_c is the gas mass-flow rate from the compressor-scroll outlet to the turbine-scroll inlet. This mass-flow-rate difference was accounted for in the recuperator calculations (eq. (C36)). The bleed flow was also assumed to reduce the effective turbine-inlet temperature by

$$\Delta(T_1) = \frac{0.01(T_1 - T_5)}{0.99} \quad (C27)$$

such that

$$T_1' = T_1 - \Delta(T_1) \quad (C28)$$

The author feels that this penalty (eq. (C27)) is conservative and should compensate for both bleed-flow penalties.

Windage loss. - Alternator windage was assumed to vary as (see ref. 8),

$$\frac{L_w}{L_w^*} = \left(\frac{Re}{Re^*} \right)^n \left(\frac{\rho}{\rho^*} \right) \left(\frac{N}{N^*} \right)^3 \quad (C29)$$

Then, for an ideal gas,

$$\rho \propto \frac{M_w p}{T}$$

and, for fixed geometry,

$$Re \propto \frac{m}{\mu}$$

Hence, assuming constant-temperature operation, or $T^* = T$,

$$\frac{L_w}{L_w^*} = \left(\frac{m}{m^*} \right)^n \left(\frac{\mu^*}{\mu} \right)^n \left(\frac{M_w}{M_w^*} \right) \left(\frac{p}{p^*} \right) \left(\frac{N}{N^*} \right)^3 \quad (C30)$$

and for choked flow, $m \propto p$; therefore,

$$\frac{L_w}{L_w^*} = \left(\frac{m}{m^*} \right)^{n+1} \left(\frac{\mu^*}{\mu} \right)^n \left(\frac{M_w}{M_w^*} \right) \left(\frac{N}{N^*} \right)^3 \quad (C31)$$

When equation (C31) and design predictions for windage losses were used, $n = -0.40$ was found to give an acceptable fit. The design predictions for windage losses were in agreement with later test results (ref. 4). The reference or starred conditions in equation (C31) were evaluated at the 10-kilowatt gross output conditions and for operation at

860° R (480 K). Hence, the expression was

$$\left. \begin{aligned} L_w &= 0.660 \left(\frac{m_h}{1.28} \right)^{0.60} \left(\frac{\mu}{2.49 \times 10^{-5}} \right)^{0.40} \left(\frac{M_w}{83.8} \right) \left(\frac{N}{36000} \right)^3 \\ L_w &= 0.660 \left(\frac{m_h}{0.581} \right)^{0.60} \left(\frac{\mu}{3.71 \times 10^{-5}} \right)^{0.40} \left(\frac{M_w}{83.8} \right) \left(\frac{N}{3770} \right)^3 \end{aligned} \right\} \quad (C32)$$

Bearing friction. - Both journal- and thrust-bearing friction losses were assumed to vary as (ref. 12)

$$\frac{L_b}{L_b^*} = \left(\frac{\mu}{\mu^*} \right) \left(\frac{N}{N^*} \right)^2 \quad (C33)$$

Hence, this approximation assumed no change in total bearing loss with pressure or power level. The author believes this to be a reasonable first-order approximation. Based on design estimates, $L_b^* = 0.27$ kilowatt. And μ^* was evaluated at 860° R (480 K) for the design gas mixture. Therefore,

$$\left. \begin{aligned} L_b &= 0.27 \left(\frac{\mu}{2.49 \times 10^{-5}} \right) \left(\frac{N}{36000} \right)^2 \\ L_b &= 0.27 \left(\frac{\mu}{3.71 \times 10^{-5}} \right) \left(\frac{N}{3770} \right)^2 \end{aligned} \right\} \quad (C34)$$

Since N was constant for the results presented herein, the bearing friction loss changed only with a change from the design gas mixture.

Heat-Transfer Models

Approximate relations were developed for the recuperator and waste heat exchanger. Empirical exponents were found by fitting these models to design predictions. The models were then modified to reflect changes based on acceptance test data. For the

results presented in this report, it was assumed that the source heat exchanger could be run hot enough to attain all conditions studied.

Recuperator. - Recuperator heat-transfer effectiveness is a function of the gas mass-flow rate and the heat to be transferred. For the purpose of constructing a model, the difference in gas mass-flow rates (eq. (C26)) was neglected. After E_r was determined, the recuperator-outlet temperatures, including the flow difference, were calculated from

$$T_6 = T_5 + E_r(T_2 - T_5) \quad (C35)$$

and

$$T_3 = T_2 - \frac{m_c}{m_h} (T_6 - T_5) \quad (C36)$$

The heat to be transferred is given by

$$Q \propto m c_p (T_2 - T_3) \quad (C37)$$

and by

$$Q \propto U A (T_3 - T_5) \quad (C38)$$

Ratioing and combining yielded

$$\frac{Q}{Q^*} = \frac{m c_p (T_2 - T_3)}{m^* c_p^* (T_2^* - T_3^*)} = \frac{U (T_3 - T_5)}{U^* (T_3^* - T_5^*)} \quad (C39)$$

But, from equations (C35) and (C36),

$$\frac{T_2 - T_3}{T_3 - T_5} = \frac{E_r}{1 - E_r} \quad (C40)$$

Therefore,

$$\frac{E_r}{1 - E_r} = \left(\frac{U}{U^*} \right) \left(\frac{m^*}{m} \right) \left(\frac{c_p^*}{c_p} \right) \left(\frac{E_r^*}{1 - E_r^*} \right) \quad (C41)$$

From reference 13, when the small terms due to wall conduction and fouling factors were neglected,

$$\frac{1}{U_h} = \frac{1}{\eta_{s,h} h_h} + \frac{1}{\left(\frac{A_c}{A_h} \right) \eta_{s,c} h_c} \quad (C42)$$

Assuming $\eta_{s,h} = \eta_{s,c} \cong 1$ and $h_h \cong h_c$ yields

$$U_h = h_h \left(\frac{1}{1 + \frac{A_c}{A_h}} \right) \quad (C43)$$

Therefore,

$$U \propto h \quad (C44)$$

The expression for the local-heat-transfer coefficient may be written from the definition of the Colburn factor j as

$$h = j G c_p (Pr)^{-2/3} \quad (C45)$$

where for constant γ and fixed geometry,

$$j \propto (Re)^n \quad (\text{ref. 13}) \quad (C46)$$

$$G \propto m \quad (C47)$$

$$Re \propto \frac{m}{\mu} \quad (C48)$$

$$c_p \propto \frac{1}{M_w} \quad (C49)$$

and

$$Pr \propto \frac{\mu}{kM_w} \quad (C50)$$

Therefore,

$$\frac{h}{h^*} = \frac{U}{U^*} = \left(\frac{m}{m^*} \right)^{n+1} \left(\frac{\mu^*}{\mu} \right)^{n+2/3} \left(\frac{k}{k^*} \right)^{2/3} \left(\frac{M_w^*}{M_w} \right)^{1/3} \quad (C51)$$

Substitution of equation (C51) into equation (C41) yielded

$$\frac{E_r}{1 - E_r} = \left(\frac{m}{m^*} \right)^n \left(\frac{M_w}{M_w^*} \right)^{2/3} \left(\frac{k}{k^*} \right)^{2/3} \left(\frac{\mu^*}{\mu} \right)^{n+2/3} \left(\frac{E_r^*}{1 - E_r^*} \right) \quad (C52)$$

Recuperator design predictions were used in equation (C52) to solve for n . A value of $n = -0.48$ was found to fit the predictions. The predicted changes were verified during the recuperator air acceptance tests. However, a value $E_r^* = 0.941$ was projected rather than the design value of 0.95 given in table I. When $E_r^* = 0.941$ was used, the expression became

$$\left. \begin{aligned} \frac{E_r}{1 - E_r} &= 15.95 \left(\frac{M_h}{1.28} \right)^{-0.48} \left(\frac{M_w}{83.8} \right)^{2/3} \left(\frac{k}{7.22 \times 10^{-6}} \right)^{2/3} \left(\frac{3.25 \times 10^{-5}}{\mu} \right)^{0.19} \\ \frac{E_r}{1 - E_r} &= 15.95 \left(\frac{M_h}{0.581} \right)^{-0.48} \left(\frac{M_w}{83.8} \right)^{2/3} \left(\frac{k}{0.0450} \right)^{2/3} \left(\frac{484 \times 10^{-5}}{\mu} \right)^{0.19} \end{aligned} \right\} \quad (C53)$$

where the reference or starred conditions (eq. (C52)) were evaluated at the flow conditions for 10 kilowatts of gross power output. The gas properties were evaluated at

$$\bar{T} = \frac{T_2 + T_5}{2} \quad (C54)$$

Waste heat exchanger. - A slightly different approach was taken for the waste heat exchanger. Its heat-transfer effectiveness is a function of both the gas and liquid mass-flow rates, the specific heats, and the heat to be transferred. Expressed functionally,

$$E_w = f'(C_w, N_{tu}) \quad (C55)$$

where

$$C_w \equiv \frac{mc_p}{\left(\frac{mc_p}{l}\right)_l} \quad (C56)$$

and

$$N_{tu} \equiv \frac{UA}{\left(\frac{mc_p}{l}\right)_m} = \frac{UA}{mc_p} \quad (C57)$$

After E_w was determined, the liquid-side temperatures resulted from

$$T_{4,l} = T_3 - \frac{T_3 - T_4}{E_w} \quad (C58)$$

$$T_{3,l} = T_{4,l} + C_w(T_3 - T_4) \quad (C59)$$

The local gas-side heat-transfer coefficient was assumed to vary as in equation (C51) for the recuperator. Based on the design geometry and conditions, $h_g^* = 0.00556$ Btu per second per square foot per $^{\circ}R$ ($114 \text{ J}/(\text{sec})(\text{m}^2)(\text{K})$) was calculated. From the design predictions, $n = -0.65$ was found to fit. Hence,

$$h_g = 0.00556 \left(\frac{m}{1.28} \right)^{0.35} \left(\frac{2.01 \times 10^{-5}}{\mu} \right)^{0.02} \left(\frac{83.8}{M_w} \right)^{1/3} \left(\frac{k}{4.77 \times 10^{-6}} \right)^{2/3} \quad \left. \right\} \quad (C60)$$

$$h_g = 114 \left(\frac{m}{0.581} \right)^{0.35} \left(\frac{3.00 \times 10^{-5}}{\mu} \right)^{0.02} \left(\frac{83.8}{M_w} \right)^{1/3} \left(\frac{k}{0.0298} \right)^{2/3} \quad \left. \right\}$$

where the reference or starred conditions (eq. (C52)) were evaluated at the flow conditions for 10 kilowatts of gross power output. The gas properties were evaluated at

$$\bar{T} = \frac{T_3 + T_4}{2} \quad (C61)$$

The local-heat-transfer coefficient on the liquid side may be expressed by equation (C45), but in this case

$$j \propto \left[(Re)_l \right]^n \quad (C62)$$

$$(Re)_l \propto \frac{m_l}{\mu_l} \quad (C63)$$

$$G_l \propto m_l \quad (C64)$$

$$c_{p,l} = f'(\bar{T}_l) \quad (C65)$$

$$(Pr)_l = \left(\frac{c_p \mu}{k} \right)_l \quad (C66)$$

Therefore,

$$\left(\frac{h}{h^*} \right)_l = \left(\frac{m}{m^*} \right)_l^{n+1} \left(\frac{\mu^*}{\mu} \right)_l^{n+2/3} \left(\frac{c_p}{c_p^*} \right)_l^{1/3} \left(\frac{k}{k^*} \right)_l^{2/3} \quad (C67)$$

The exponent n was assumed to be the same for both surfaces, and for the design conditions,

$$h_l^* = 0.0137 \frac{\text{Btu}}{(\text{sec})(\text{ft}^2)(^{\circ}\text{R})}$$

$$= 281 \frac{\text{J}}{(\text{sec})(\text{m}^2)(\text{K})}$$

was calculated. Changes in k_l and μ_l were neglected, and the expression was simplified to

$$\left. \begin{aligned} h_l &= 0.0137 \left(\frac{m_l c_{p,l}}{0.0870} \right)^{0.35} \\ h_l &= 281 \left(\frac{m_l c_{p,l}}{165} \right) \end{aligned} \right\} \quad (C68)$$

where the liquid capacity rate was evaluated at design C_w , and $c_{p,l}$ is evaluated at

$$\bar{T}_l = \frac{T_{3,l} + T_{4,l}}{2} \quad (C69)$$

After h_l and h_g are calculated, the procedure to find E_w was that of Kays and London (ref. 13). The crossflow equations for "unmixed" liquid flow and "mixed" gas flow were used. For completeness, the equations, with substitutions for the design geometry, are presented. The overall gas-side heat-transfer coefficient results from

$$\frac{1}{U_g} = \frac{1}{\eta_{s,g} h_g} + \frac{1}{0.336 \eta_{s,l} h_l} \quad (C70)$$

where

$$\eta_{s,g} = 1 - 0.682(1 - \eta_{f,g}) \quad (C71)$$

with

$$\left. \begin{aligned} \eta_{f,g} &= \frac{\tan h(0.268 \sqrt{h_g})}{0.268 \sqrt{h_g}} \\ \eta_{f,g} &= \frac{\tan h(0.00337 \sqrt{h_g})}{0.00337 \sqrt{h_g}} \end{aligned} \right\} \quad (C72)$$

and where

$$\eta_{s,l} = 1 - 0.510(1 - \eta_{f,l}) \quad (C73)$$

with

$$\left. \begin{aligned} \eta_{f,l} &= \frac{\tan h(0.076 \sqrt{h_l})}{0.076 \sqrt{h_l}} \\ \eta_{f,l} &= \frac{\tan h(0.000957 \sqrt{h_l})}{0.000957 \sqrt{h_l}} \end{aligned} \right\} \quad (C74)$$

The number of thermal units was then evaluated from

$$N_{tu} = \frac{\varphi (UA)_g^*}{mc_p} \quad (C75)$$

where

$$\varphi \equiv \frac{(UA)_g}{(UA)_g^*} = 0.93 \quad (C76)$$

based on the air acceptance test results; and from the design, $A_g = 405$ square feet (37.6 m^2). Since there are eight liquid passes,

$$N_{tu,p} = \frac{N_{tu}}{8} \quad (C77)$$

Then,

$$\Gamma_p = 1 - e^{-C_w N_{tu,p}} \quad (C78)$$

$$E_p = 1 - e^{-\Gamma_p / C_w} \quad (C79)$$

$$\xi \equiv \frac{1 - C_w E_p}{1 - E_p} \quad (C80)$$

and

$$E_w = \frac{\xi^8 - 1}{\xi^8 - C_w} \quad (C_w \neq 1) \quad (C81)$$

If $C_w = 1$, by L'Hospital's rule,

$$E_w = \frac{8E_p}{1 + 7E_p} \quad (C82)$$

Gas Pressure Drops

For each heat exchanger, the change in total-pressure drop was assumed to vary as the change in core friction pressure drop. The following proportionalities lead to the relation in equation (C89):

$$\frac{\Delta p}{p} \propto \frac{f \rho v^2}{p} \quad (C83)$$

where

$$f \propto (Re)^n \propto \left(\frac{m}{\mu}\right)^n \quad (C84)$$

and

$$v \propto \frac{m}{\rho} \quad (C85)$$

Therefore,

$$\frac{\Delta p}{p} \propto \left(\frac{m}{\mu} \right)^n \left(\frac{\rho}{p} \right) \left(\frac{m}{\rho} \right)^2 \quad (C86)$$

But

$$\rho \propto \frac{M_w p}{T} \quad (C87)$$

and

$$\frac{\Delta p}{p} \propto \frac{m^n T}{\mu^n M_w} \left(\frac{m}{p} \right)^2 \quad (C88)$$

Hence, the general expression used for each heat exchanger was

$$\left(\frac{\Delta p}{p} \right) = \left(\frac{m}{m^*} \right)^{n+2} \left(\frac{\mu^*}{\mu} \right)^n \left(\frac{M_w^*}{M_w} \right) \left(\frac{T}{T^*} \right) \left(\frac{p^*}{p} \right)^2 \left(\frac{\Delta p}{p} \right)^* \quad (C89)$$

All values of $(\Delta p/p)^*$ used in the analysis were based on the total design values. Air measurements have shown smaller values in some cases. However, for conservatism, the design numbers were used. Viscosity terms were evaluated at the average temperature through the component. However, temperature and pressure were evaluated, conservatively, at the inlet conditions of the component.

Recuperator. - A value of $n = -0.60$ was found to fit the design predictions. All reference or starred values (eq. (C89)) were evaluated at the flow conditions estimated to give 10 kilowatts of gross output, in the following equations:

$$\left. \begin{aligned} \left(\frac{\Delta p}{p} \right)_{r,h} &= 0.022 \left(\frac{m_h}{1.28} \right)^{1.40} \left(\frac{3.30 \times 10^{-5}}{\bar{\mu}} \right)^{-0.60} \left(\frac{T_2}{1690} \right) \left(\frac{83.8}{M_w} \right) \left(\frac{23.5}{p_2} \right)^2 \\ \left(\frac{\Delta p}{p} \right)_{r,h} &= 0.022 \left(\frac{m_h}{0.581} \right)^{1.40} \left(\frac{4.91 \times 10^{-5}}{\bar{\mu}} \right)^{-0.60} \left(\frac{T_2}{939} \right) \left(\frac{83.8}{M_w} \right) \left(\frac{162}{p_2} \right)^2 \end{aligned} \right\} \quad (C90)$$

$$\left. \begin{aligned} \left(\frac{\Delta p}{p} \right)_{r, c} &= 0.011 \left(\frac{m_c}{1.267} \right)^{1.40} \left(\frac{3.20 \times 10^{-5}}{\bar{\mu}} \right)^{-0.60} \left(\frac{T_5}{738} \right) \left(\frac{83.8}{M_w} \right) \left(\frac{43.3}{p_5} \right)^2 \\ \left(\frac{\Delta p}{p} \right)_{r, c} &= 0.011 \left(\frac{m_c}{0.575} \right)^{1.40} \left(\frac{4.77 \times 10^{-5}}{\bar{\mu}} \right)^{-0.60} \left(\frac{T_5}{410} \right) \left(\frac{83.8}{M_w} \right) \left(\frac{297}{p_5} \right)^2 \end{aligned} \right\} \quad (C91)$$

Waste heat exchanger. - The same value, $n = -0.60$, was found to fit the design predictions. All reference or starred values (eq. (C89)) were evaluated at the flow conditions for 10 kilowatts gross output in the following equations:

$$\left. \begin{aligned} \left(\frac{\Delta p}{p} \right)_{w, g} &= 0.0073 \left(\frac{m_h}{1.28} \right)^{1.40} \left(\frac{2.02 \times 10^{-5}}{\bar{\mu}} \right)^{-0.60} \left(\frac{T_5}{795} \right) \left(\frac{83.8}{M_w} \right) \left(\frac{23.0}{p_3} \right)^2 \\ \left(\frac{\Delta p}{p} \right)_{w, g} &= 0.0073 \left(\frac{m_h}{0.581} \right)^{1.40} \left(\frac{3.01 \times 10^{-5}}{\bar{\mu}} \right)^{-0.60} \left(\frac{T_3}{442} \right) \left(\frac{83.8}{M_w} \right) \left(\frac{158}{p_3} \right)^2 \end{aligned} \right\} \quad (C92)$$

Source heat exchanger. - For this heat exchanger, a value of $n = -0.20$ was used in its design analysis. The same value was used in this analysis. The reference or starred values were estimated for the 10-kilowatt-output conditions and were rounded off. The expression, as used in the program, was

$$\left. \begin{aligned} \left(\frac{\Delta p}{p} \right)_{so} &= 0.022 \left(\frac{m_h}{1.3} \right)^{1.8} \left(\frac{4.52 \times 10^{-5}}{\bar{\mu}} \right)^{-0.20} \left(\frac{T_6}{1650} \right) \left(\frac{83.8}{M_w} \right) \left(\frac{43.8}{p_6} \right)^2 \\ \left(\frac{\Delta p}{p} \right)_{so} &= 0.022 \left(\frac{m_h}{0.59} \right)^{1.8} \left(\frac{6.74 \times 10^{-5}}{\bar{\mu}} \right)^{-0.20} \left(\frac{T_6}{917} \right) \left(\frac{83.8}{M_w} \right) \left(\frac{302}{p_6} \right)^2 \end{aligned} \right\} \quad (C93)$$

Ducting. - The friction pressure drop for ducting may be expressed as

$$\frac{\Delta p}{p} = \frac{K_{eq} f \rho v^2}{2 g p} \quad (C94)$$

or, as used in the program

$$\left. \begin{aligned} \frac{\Delta p}{p} &= K_{eq} f \left(\frac{1545}{M_w} \right) \left(\frac{T}{2g} \right) \left(\frac{G}{p} \right)^2 \\ \frac{\Delta p}{p} &= K_{eq} f \left(\frac{8317}{M_w} \right) \left(\frac{T}{2g} \right) \left(\frac{G}{p} \right)^2 \end{aligned} \right\} \quad (C95)$$

The following friction factors were used:

$$f = \frac{16}{Re} \quad \text{for } Re \leq 6000 \text{ (laminar flow)} \quad (C96)$$

and

$$f = \frac{0.316}{(Re)^{0.25}} \quad \text{for } Re > 6000 \quad (C97)$$

which is the Blasius formula for turbulent flow (ref. 14).

Values for K_{eq} for each segment of the ducting were calculated from equations (C95) for the design pressure drops allowed at the 10-kilowatt-output conditions. These values are shown in table II.

TABLE II. - VALUES OF K_{eq}

Ducting from-	Equivalent duct length-to-diameter ratio, K_{eq} , dimensionless
Turbine to recuperator	47.2
Waste heat exchanger to compressor	38.8
Compressor to recuperator	42.0
Recuperator to source heat exchanger	136.0
Source heat exchanger to turbine	87.5

Gas Inventory

For the calculation of total inventory, the gas loop was divided into nine segments. The inventory was calculated as

$$W_g = \frac{144 M_w}{1545} \sum_{i=1}^9 \left(\frac{\bar{p}V}{T} \right)_i \quad \left. \right\} \quad (C98)$$

$$W_g = \frac{M_w}{8317 \times 10^3} \sum_{i=1}^9 \left(\frac{\bar{p}V}{T} \right)_i \quad \left. \right\}$$

The segments and their estimated gas volumes are shown in table III.

TABLE III. - ESTIMATED VOLUMES OF
GAS-LOOP SEGMENTS

Segment	Volume, V	
	ft ³	m ³
Duct from turbine to recuperator	0.326	0.00923
Recuperator, hot side	1.98	.0560
Waste heat exchanger	.714	.0202
Duct from waste heat exchanger to compressor	.104	.00294
Duct from compressor to recuperator	.123	.00348
Recuperator, cold side	1.27	.0359
Duct from recuperator to source heat exchanger	.184	.00521
Source heat exchanger	.380	.0108
Duct from source heat exchanger to turbine	.370	.0105
Total	5.451	0.1543

System Electrical Needs

Part of the gross alternator power output $P_{a,G}$ is used to control the power system itself. Hence, the gross system output power is given by

$$P_{sy,G} = P_{a,G} - P_e \quad (C99)$$

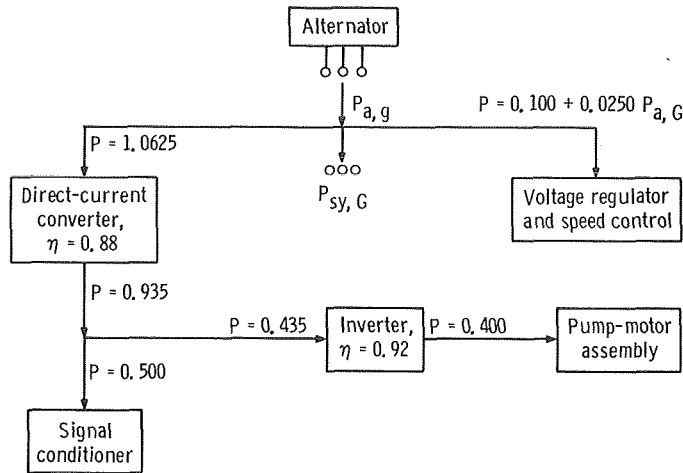


Figure 12. - Schematic diagram of estimated system power needs.

The estimated system power needs are shown in figure 12. Hence, the expression for control power is

$$P_e = 1.1625 + 0.0250 P_{a, G} \quad (C100)$$

All of the electrical component power needs are based on approximations. The power required by the pump-motor assembly is a function of liquid mass-flow rate. Measured acceptance test results show this motor power need to vary between 330 to 430 watts. The use of 400 watts would correspond to a total coolant-flow rate of 0.35 pound mass per second (0.16 kg/sec).

Radiator Areas

In the analysis of parametric system operation, approximate values of prime radiator area are calculated. Over the range of pump design mass-flow rates, the calculated pump-motor coolant-temperature rise varied from about 0.5 to 1.5 R^o. For conservatism, a constant temperature rise of 2 R^o (1 K) was assumed. Then, neglecting any temperature drop between the liquid and the radiator surface,

$$T_{R, i} = T_{3, l} \quad (C101)$$

and

$$\left. \begin{aligned} T_{R,o} &= T_{4,l} - 2 \\ T_{R,o} &= T_{4,l} - 1 \end{aligned} \right\} \quad (C102)$$

The prime, or minimum area, need was then calculated from

$$A_p = \frac{(mc_p)_l}{4\sigma\epsilon T_S^3} \left\{ \ln \frac{(T_{R,i} - T_S)(T_{R,o} + T_S)}{(T_{R,o} - T_S)(T_{R,i} + T_S)} - 2 \left[\tan^{-1} \left(\frac{T_{R,i}}{T_S} \right) - \tan^{-1} \left(\frac{T_{R,o}}{T_S} \right) \right] \right\} \quad (C103)$$

This expression is a simplified form of the general expression presented in reference 15. The missing term, which adds the effect of the coolant heat-transfer coefficient, has been assumed to be small. Mathematically, this is true only for an infinite heat-transfer coefficient.

REFERENCES

1. Klann, John L.: Analysis and Selection of Design Conditions for a Radioisotope Brayton-Cycle Space Powerplant. NASA TN D-4600, 1968.
2. Klann, John L.: 2 to 10 Kilowatt Solar or Radioisotope Brayton Power System. Intersociety Energy Conversion Engineering Conference. Vol. I. IEEE, 1968, pp. 407-415.
3. Nusbaum, William J.; and Kofskey, Milton G.: Cold Performance Evaluation of 4.97-Inch Radial-Inflow Turbine Designed for Single-Shaft Brayton Cycle Space-Power System. NASA TN D-5090, 1969.
4. Repas, David S.; and Edkin, Richard A.: Performance Characteristics of a 14.3-Kilovolt-Ampere Modified Lundell Alternator for 1200 Hertz Brayton-Cycle Space-Power System. NASA TN D-5405, 1969.
5. Wong, R. Y.; Klassen, Hugh; Evans, R. C.; and Winzig, C.: Experimental Investigation of a Single Shaft Turbine-Compressor-Alternator Unit Operating as Part of a Brayton Power Generation System. NASA TM X-1869, 1969.
6. Meyer, Sheldon J.; and Evans, Robert C.: Preliminary Performance of a 1200 Hertz Alternator, Voltage Regulator, and Electronic Speed Control Operating in a Brayton Cycle Power System. NASA TM X-52645, 1969.
7. McKhann, G. G.: Preliminary Design of a Pu-238 Isotope Brayton Cycle Power System for MORL. Vol. I: Technical Summary. Rep. SM-48832, Douglas Aircraft Co., Inc. (NASA CR-68809), Sept. 1965.
8. Shepherd, D. G.: Principles of Turbomachinery. The Macmillan Co., 1956.
9. Bernatowicz, Daniel T.: NASA Solar Brayton Cycle Studies. Paper presented at the Symposium on Solar Dynamics Systems, Solar and Mechanics Working Groups of the Interagency Advanced Power Group, Washington, D.C., Sept. 24-25, 1963.
10. Vanco, Michael R.: Analytical Comparison of Relative Heat-Transfer Coefficients and Pressure Drops of Inert Gases and Their Binary Mixtures. NASA TN D-2677, 1965.
11. Scarborough, James B.: Numerical Mathematical Analysis. Second ed., The Johns Hopkins Press, 1950.
12. Gunter, Edgar J., Jr.; Hinkle, James G.; and Fuller, Dudley D.: Design Guide for Gas-Lubricated Tilting-Pad Journal and Thrust Bearings with Special Reference to High-Speed Rotors. Rep. NY02512-1, Franklin Institute Research Lab., Nov. 1964.

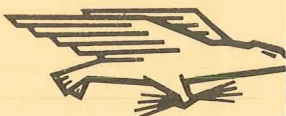
13. Kays, W. M.; and London, A. L.: *Compact Heat Exchangers*. Second ed., McGraw-Hill Book Co., Inc., 1964.
14. Streeter, Victor L.: *Fluid Mechanics*. Second ed., McGraw-Hill Book Co., Inc., 1958.
15. Glassman, Arthur, J.: *Thermodynamic and Turbomachinery Concepts for Radioisotope and Reactor Brayton-Cycle Space Power Systems*. NASA TN D-2968, 1965.

NATIONAL AERONAUTICS AND SPACE ADMINISTRATION

WASHINGTON, D. C. 20546

OFFICIAL BUSINESS

FIRST CLASS MAIL



POSTAGE AND FEES PAID
NATIONAL AERONAUTICS AND
SPACE ADMINISTRATION

POSTMASTER: If Undeliverable (Section 15:
Postal Manual) Do Not Retu

"The aeronautical and space activities of the United States shall be conducted so as to contribute . . . to the expansion of human knowledge of phenomena in the atmosphere and space. The Administration shall provide for the widest practicable and appropriate dissemination of information concerning its activities and the results thereof."

— NATIONAL AERONAUTICS AND SPACE ACT OF 1958

NASA SCIENTIFIC AND TECHNICAL PUBLICATIONS

TECHNICAL REPORTS: Scientific and technical information considered important, complete, and a lasting contribution to existing knowledge.

TECHNICAL NOTES: Information less broad in scope but nevertheless of importance as a contribution to existing knowledge.

TECHNICAL MEMORANDUMS: Information receiving limited distribution because of preliminary data, security classification, or other reasons.

CONTRACTOR REPORTS: Scientific and technical information generated under a NASA contract or grant and considered an important contribution to existing knowledge.

TECHNICAL TRANSLATIONS: Information published in a foreign language considered to merit NASA distribution in English.

SPECIAL PUBLICATIONS: Information derived from or of value to NASA activities. Publications include conference proceedings, monographs, data compilations, handbooks, sourcebooks, and special bibliographies.

TECHNOLOGY UTILIZATION PUBLICATIONS: Information on technology used by NASA that may be of particular interest in commercial and other non-aerospace applications. Publications include Tech Briefs, Technology Utilization Reports and Notes, and Technology Surveys.

Details on the availability of these publications may be obtained from:

SCIENTIFIC AND TECHNICAL INFORMATION DIVISION

NATIONAL AERONAUTICS AND SPACE ADMINISTRATION

Washington, D.C. 20546